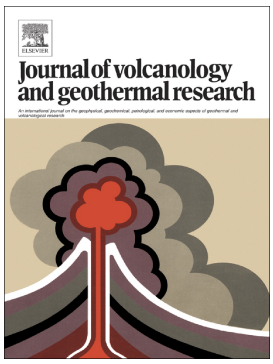

Amphibole record of the 1964 plinian and following dome-forming eruptions of Shiveluch volcano, Kamchatka

Natalia Gorbach, Tatiana Philosofova, Maxim Portnyagin

PII: S0377-0273(20)30373-5

DOI: https://doi.org/10.1016/j.jvolgeores.2020.107108

Reference: VOLGEO 107108

To appear in: *Journal of Volcanology and Geothermal Research*

Received date: 14 July 2020

Revised date: 29 October 2020

Accepted date: 30 October 2020

Please cite this article as: N. Gorbach, T. Philosofova and M. Portnyagin, Amphibole record of the 1964 plinian and following dome-forming eruptions of Shiveluch volcano, Kamchatka, *Journal of Volcanology and Geothermal Research* (2020), https://doi.org/10.1016/j.jvolgeores.2020.107108

Amphibole record of the 1964 plinian and following dome-forming eruptions of Shiveluch volcano, Kamchatka

Natalia Gorbach[1,*] n_gorbach@mail.ru, Tatiana Philosofova[1], Maxim Portnyagin[2,3]

[1]Institute of Volcanology and Seismology, Petropavlovsk-Kamchatsky, Russia

[2]GEOMAR Helmholtz Centre for Ocean Research Kiel, Kiel, Germany

[3]Vernadsky Institute of Geochemistry and Analytical Chemistry, Moscow, Russia

[*]Corresponding author.

Abstract

Shiveluch is one of the most active explosive volcanoes worldwide. During the last plinian eruption in 1964 and the following (1980-current time) dome-forming eruptions Shiveluch has produced andesites and dacites (SiO_2~60-64 wt.%) containing variably zoned, compositionally and texturally diverse amphibole phenocrysts. In this work, we attempt to decode the complex zoning of the amphibole crystals in the 55-year series of pumice, dome rocks and mafic enclaves in order to reconstruct the most recent evolution of the volcano plumbing system.

The amphibole zoning in Shiveluch andesites reveals correlation with the style and date of eruption. High-Al cores mantled by low-Al rims in amphiboles from the 1964 plinian eruption record a drastic decrease of pressure and rapid magma ascent from the lower crust to the shallow magma chamber. Typically unzoned and often opacitized low-Al crystals from the early dome-building episodes in 1980-1981 and 1993-1995 reflect magma crystallization in the shallow magma chamber. Complexly zoned amphiboles from andesites erupted in 2000s indicate replenishment of the shallow magma chamber with mafic magma and syn-eruptive mixing processes. Amphibole-based barometric calculations obtained by different approaches indicate that the Shiveluch plumbing system is complex and comprises two, mafic and silicic magma storage zones at ~15-20 km and ~5-6 km depths. We suggest that both

episodes of the plinian eruption in 1964 and the extensive dome growth in 2001-2016 were driven by influx of mafic magma in the shallow storage zone beneath Shiveluch. The mafic replenishment likely preceded the 1964 plinian eruption and repeatedly occurred during the period of extensive dome growth in 2001-2016. The variable styles of the recent Shiveluch eruptions may be controlled by the relative volume of the mafic recharges and their thermal and viscosity effects on the efficiency of magma mixing.

Keywords: *andesite, Shiveluch, Kamchatka, amphibole, thermobarometry*

1. Introduction

The knowledge of volcano plumbing system and physicochemical conditions in magmas prior to eruption is crucial for prediction of transition from dome-building effusive to explosive eruption of andesitic volcanoes and for assessment of the associated volcanic risks (e.g., Eichelberger, 1995; Ruprecht and Bachmann, 2010; Cassidy et al., 2018; Auer et al., 2018). Chemical zoning of minerals is a diary of the changeable magmatic conditions preceding eruption and, therefore, its decoding provides an effective tool for the reconstruction of the pre-eruptive processes (e.g., Izbekov et al., 2002; Humphreys et al., 2006; Ginibre et al., 2007; Streck, 2008; Ruprecht et al., 2012; Churikova et al., 2013). Amphibole is one of the most informative minerals for such studies due to its common occurrence in water-rich arc andesite and dacite magmas and high sensitivity of its composition to temperature, pressure, oxygen fugacity and melt composition (e.g., Spear, 1981; Johnson and Rutherford, 1989; Holland and Blundy, 1994; Scaillet and Evans, 1999; Almeev et al., 2002; Rutherford and Devine, 2003; Ridolfi et al., 2010; Krawczynski et al., 2012; Kiss et al., 2014; Putirka et al., 2016). Numerous recent studies demonstrated the effectiveness of using amphibole composition for the reconstruction of magma evolution beneath dome-forming volcanoes such as Merapi, Indonesia (Erdman et al., 2014), Mount St.

Helens and Augustine, USA (Thornber et al., 2008; Wanke et al., 2018; Humphreys et al., 2019; De Angelis et al., 2013), Soufrie`re Hills (Monserrat) (Humphreys et al., 2009a); Unzen, Japan (Sato et al., 2005), Bezymianny, Kamchatka, Russia (Turner et al., 2013).

Shiveluch is the most productive and highly explosive volcano on the Kamchatka Peninsula and one of the most active dome-building volcanoes worldwide. The drastic predominance of amphibole-bearing andesites at all stages of volcanic evolution since the Late Pleistocene until present distinguishes Shiveluch among the other Kamchatka volcanoes (e.g., Melekestsev et al., 1991; Volynets et al., 1997; Ponomareva et al., 2007; 2015; Gorbach et al., 2013). Catastrophic plinian eruptions alternating with lava dome growth accompanied by voluminous pyroclastic flows, debris avalanches, lahars and ash falls are the typical features of Shiveluch eruptive style in the last 10 ka (Ponomareva et al., 2007). The historic record includes two plinian eruptions (February 1854 and November 1964) alternated by lava dome growth (Melekestsev et al., 2004). Since 1980, the growing lava dome has been producing andesites and dacites containing amphibole phenocrysts with highly variable compositional and textural patterns, which reflect the complexity of magmatic processes occurring under Shiveluch (Dirksen et al., 2006; Humphreys et al., 2006; Gorbach et al., 2016). Because of frequent eruptions and the common occurrence of amphibole, the Shiveluch eruptive sequence provides an excellent opportunity for better understanding the nature of shallow magmatic processes leading to highly active and explosive andesitic arc volcanism.

In this work, we combine volcanological observations with chemical and textural analysis of amphibole phenocrysts for a time-series from the 1964 plinian eruption and the following stage of lava dome growth (1980-present). The erupted pumiceous rocks from pyroclastic flows, dome forming lavas and mafic enclaves were studied. We show that the heterogeneity of Shiveluch amphiboles originates from mixing of evolved and more primitive magmas in a shallow magma chamber and also reflects the presence of amphiboles

crystallized at deeper depths from water-rich mafic magmas. Our results testify a complex architecture of the Shiveluch plumbing system, which includes deep mafic and shallow silicic magma storage zones in the crust.

2. Shiveluch volcanic history

Shiveluch volcano is the northernmost active volcano in Kamchatka. It is situated in the northern part of the Central Kamchatka depression close to the edge of the subducting Pacific plate at the Kurile–Kamchatka and Aleutian arc junction (Figs.1a, 1b). The estimated magma discharge, assuming the volcano age of 60-70 ka, is close to 36×10^6 tons per year that is an order of magnitude higher than that for a typical island arc volcano (Melekestsev et al., 1991). The volcanic edifice has a volume of ~1000 km^3 and comprises partly destroyed Late Pleistocene Old Shiveluch stratovolcano and Holocene Young Shiveluch eruptive center (Fig. 1c). Old Shiveluch activity included two clearly defined stages. The early stage was essentially explosive and produced a 1800-2000 m thick pile of coarse pyroclastic deposits (pyroclastic flows, volcanic breccias and tephra), while the late stage was effusive and generated thick, mainly andesitic lava flows (Menyailov, 1955; Melekestsev et al., 1991; Gorbach et al., 2013). A large sector collapse, which occurred before the Last Glacial Maximum (23-24 ka BP), partially destroyed the Old Shiveluch edifice (Melekestsev et al., 1991). Recent studies (Pevzner et al. 2013; Ponomareva et al., 2015) indicate that explosive basaltic andesite eruptions took place after the sector collapse at 12-16 ka BP and associated with eruptive centers in the southwestern sector of Old Shiveluch, which is known as Baidarny Spur.

Young Shiveluch activity started at ~11 ka (Gorbach and Portnyagin, 2011; Pevzner et al., 2013). The Holocene eruptive center was nested in the northwestern part of the Old Shiveluch collapse crater and covered an area of 40 km^2. The Young Shiveluch edifice comprises fragments of old domes, lava flows, and a few dikes with the composition ranging

from high-Mg# (Mg# = Mg/(Mg + Fe^{tot}), on molar basis) basaltic andesites (SiO_2=55.0-56.7 wt. %, Mg# =0.58-0.67) to predominating more evolved andesites (SiO_2=57.3-62.5, Mg#=0.55-0.64) (Gorbach and Portnyagin, 2011). The active crater with growing lava dome (Figs. 1a, 1c) is located in the center of the Young Shiveluch edifice. Satellite Karan domes of Holocene age are situated ~5 km southwest from the active crater at the Old Shiveluch flank (Fig. 1c).

Young Shiveluch had at least sixty large eruptions in the Holocene that were large enough to be preserved in the regional tephra records (Ponomareva et al. 1998; 2007). These eruptions generated thick pyroclastic flows, debris avalanches, ash falls, and lahars distributed mostly to the south of the eruptive center, and have formed a pyroclastic sloping field with an area of nearly 400 km^2. The majority of the Holocene eruptions had a volume of 0.5-2 km^3 and their tephra beds are preserved in the regional tephra records over the distances up to ~350 km from the volcano (Ponomareva et al., 2007; 2015). Specific mineralogical and geochemical features (i.e., presence of amphibole, high-Mg and high-Cr bulk and strongly calc-alkaline medium-K glass compositions) make Young Shiveluch tephras excellent markers for dating Holocene deposits and landforms in Kamchatka (Ponomareva et al., 2007; 2015; Kyle et al., 2011; Portnyagin et al., 2020).

The two largest historic plinian eruptions occured in February 1854 and November 1964 and were separated with a period of dome growth in 1879-1883, 1928-1929 and 1944-1950 (Menyailov, 1955; Gorshkov and Dubik, 1970; Melekestsev et al., 2004).

3. The latest Shiveluch activity

3.1. 1964 eruption

The 1964 plinian eruption was one of the biggest historical explosive events in Kamchatka with respect to the volume (~0.8 km^3) of the erupted juvenile pyroclastic material. The eruption began with a failure of several lava domes in the Young Shiveluch crater and

generation of a giant debris avalanche with an area of ~100 km^2 and a volume of 1.5 km^3 (Piip, Markhinin, 1965; Tokarev, 1967; Gorshkov, Dubik, 1970; Belousov, 1995). The avalanche was followed by small-volume phreatic explosion, which ejected 0.01 km^3 of resurgent ash (Belousov, 1995). During the subsequent plinian stage of the eruption, 0.3 km^3 of pumiceous tephra and about 0.5 km^3 of pyroclastic flows deposits were erupted (Gorshkov and Dubik, 1970; Belousov, 1995).

3.2. Post-1964 activity

3.2.1. Early dome-forming episodes in 1980-81 and 1993-95

After the 1964 eruption, Shiveluch was dormant until 1980. Extrusion of viscous lava began in August 1980 without any recorded seismic precursors or preceding explosive activity (Ivanov et al., 1981). The first episode of dome growth continued until the end of 1981 and produced 0.02 km^3 of andesites (Dvigalo, 1984). In 1982, the growth stopped, and the dome exhibited only moderate fumarolic activity (Zharinov et al., 1995).

Shiveluch renewed activity in January 1993, when swarms of earthquakes with focal depth of 3-5 km and volcanic tremor were detected (Gorelchik et al., 1997). The seismic activity culminated in a powerful explosive eruption in April 1993, when the eruptive column rose 15-18 km above the sea level, and pyroclastic flows and lahars were generated (Khubunaya et al., 1995). The growth of the lava dome lasted from April 1993 to the beginning of 1995 at an average rate of 3 m^3/s (Fedotov et al., 2001; Melekestsev et al., 2004; Dirksen et al., 2006). The total volume of erupted magma during the 1993-1995 episode was estimated at 0.18 km^3 (Melekestsev et al., 2004). In 1995, the volcano entered a quiet period with only moderate fumarolic activity. Beginning from 1997, rare ash emissions with increasing frequency were observed until 2000 (Melekestsev et al., 2004).

3.2.2. Extensive lava dome growth in 2001-2016

Voluminous and nearly persistent growth of the lava dome (Fig. 2a) alternating with episodes of its destruction has occurred beginning from 2001 (e.g., Gorbach et al., 2016 and references therein). Lava dome morphology changed from blocks and spines in 2001, 2003, 2005 and 2007 to lava lobes in 2004, 2011 and 2013 (Dirksen et al., 2006; Gorbach, 2006; Ramzey et al., 2012; Zharinov, Demyanchyk, 2013; Girina et al, 2014; Shevchenko et al., 2015). The extrusion rate varied from 2 to 10-14 m^3/s until 2012 (Dirksen et al., 2006; Zharinov, Demyanchyk, 2013; Shevchenko et al., 2015).

Five strong explosive eruptions (in May 2001, May 2004, February and September 2005 and October 2010) accompanied the dome growth. These events resulted in abundant ash falls in Kluchi and Ust-Kamchatsk villages (45 km south and 80 km east from volcano, respectively). In the course of these eruptions, the dome partly collapsed, and extensive pyroclastic flows covered the valleys on the southern flank of the volcano (Fig. 1c). The runout distances of the largest pyroclastic flows in February 2005 and October 2010 were ~20 km from the active crater (Fig. 2 b, c, d) (e.g., Krippner et al., 2018). Smaller, 6-12 km-long pyroclastic flows accompanied moderate explosions in 2007, 2008, 2009, 2013, and 2016 (Fig. 2 e).

The total volume of the dome lavas and pyroclastic deposits erupted in 2001-2016 is close to 1 km^3 (Shevchenko et al. 2015; Gorbach et al., 2016), about 5 times larger than during the preceding periods of Shiveluch dome growth in 1980-1981 and 1993-1995.

4. Sampling and methods

Andesites from the 1964 plinian eruption were sampled from the outcrops which are still exposed on the southwestern foot of the volcano. The products of eruptions in the period from 1980 to 2001 are not preserved; they have been destroyed by more recent eruptive events. Yuri Dubic, Alexander Belousov and Marina Belousov provided lava samples of the early dome-building periods in 1980-1981 and 1993-1995, respectively. Sergey Khubunaya

donated rocks from pyroclastic flow produced by eruption in May 2001. For the following episodes of volcanic activity, we collected ~70 samples from the growing lava dome and its pyroclastic deposits erupted between 2003 and 2016. For eruptions in February and September 2005, in 2007, 2009, 2013, and 2016, the samples were represented by hot clasts from pyroclastic flows and collected within a few days after eruptions. Mafic inclusions (enclaves) (Fig. 2d) were collected from large blocks in the 2005 and 2013 pyroclastic flow deposits.

Whole rock major element composition of these samples have been reported in previous works (Gorbach and Portnyagin, 2011; Gorbach et al., 2016). Here we report additional data on trace elements composition of selected samples of the dome rocks, mafic enclaves, and 1964 pumices. Major element analyses of most samples were obtained by X-ray fluorescence method in GEOMAR Helmholtz Centre for Ocean Research Kiel, Germany. Trace element abundances were analyzed in solutions by inductively coupled plasma mass spectrometry (ICP-MS) at the Institute of Geosciences, University of Kiel, Germany (Garbe-Schönberg, 1993) and at Acme Analytical Laboratories Ltd., Vancouver, Canada. For the most recent 2016 andesite, major and trace element concentrations were determined by XRF and ICP-MS in the Vinogradov Institute of Geochemistry, Irkutsk, Russia. International standards AGV-1, AGV-2, BHVO-2 were analyzed in one session with Shiveluch samples in GEOMAR, Kiel University, and Vinogradov Institute of Geochemistry; SO-18, SO-19 and OREAS45EA - in the AcmeLab. The data on whole rock compositions and reference materials are presented in Table 1 and Supplementary Table B1.

Texture, composition and zoning patterns of 269 amphibole crystals from 12 representative samples were studied in polished sections and in loose crystals separated from fraction of 0.25-2 mm and mounted in epoxy stubs. Back-scattered electron (BSE) images of the amphibole crystals were obtained using a scanning electron microscope Vega 3 Tescan at the Institute of Volcanology and Seismology, Petropavlovsk-Kamchatsky. Major elements

and chlorine contents in amphibole were determined using a JEOL JXA 8200 electron microprobe equipped with five wavelength dispersive spectrometers including 3 high-sensitivity ones (2 PETH and TAPH) at GEOMAR (Kiel). The analytical conditions were 15 kV accelerating voltage, 20 nA current, electron beam focused to 1 μm and 20 s counting time for all elements. Arenal hornblende and Kakanui hornblende reference samples (Jarosewich et al. 1980) were used for calibration and monitoring data quality. Based on replicate analyses of the reference amphiboles, uncertainties of single point amphibole analyses (2σ of the mean value) are 0.40 wt.% for SiO_2, 0.40 wt.% for FeO and MgO, 0.25 wt.% for Al_2O_3, 0.15 wt.% for CaO, 0.09 wt.% for TiO_2 and Na_2O, 0.04 wt.% for K_2O. The check of stoichiometry and minor correction of the amphibole microprobe analyses were performed using the AMFORM model (Ridolfi et al., 2018).

In addition to amphibole phenocrysts, the composition of coexisting plagioclase (phenocrysts, microlites and inclusions in amphibole) and pyroxenes were analyzed at the analytical conditions similar to those used those used for amphibole and using appropriate natural reference materials for plagioclase and pyroxene (Jarosevich et al., 1980). Matrix glass was analysed following protocol described by Portnyagin et al. (2020). Published data on melt inclusions and matrix glasses were used after Tolstykh et al. (1998; 2003), Humphreys et al. (2006; 2008) and Ponomareva et al. (2015). Compositions of olivine and chromium spinel from mafic enclaves were published by Gorbach and Portnyagin (2011).

5. Whole rock composition

5.1 Andesite petrography and mineral composition

The 1964 pumice contains no more than 15-20 vol. % phenocrysts (5-7 % amphibole and 10-13 % plagioclase) or their broken fragments (Fig. 3a). Highly vesiculated pumice glass is mainly microlite-free. The lava dome andesites are rich in phenocrysts and typically contain

up to 45 vol.% phenocrysts (10–30 vol. % of plagioclase and 6-15 vol. % of amphibole) in well crystallized variably vesicular groundmass (Figs. 3b, 3c).

Plagioclase (*Pl*) and amphibole (*Amp*) phenocrysts (here and thereafter mineral abbreviations are given after Whitney, Evans (2010)) from dome rocks are represented by several populations, which differ by size, texture, chemical composition, and type of zonation. The compositional range of *Pl* phenocrysts and diversity of its zoning were described in detail for the 2001 andesites (Humphreys et al., 2006), as well as for lavas of subsequent eruptions (Gorbach, 2006; Gorbach et al., 2016). The cores of *Pl* phenocrysts range from $An_{83–88}$ to An_{30}, rims and microlites are An_{48-25}. Oscillatory-zoned andesine crystals An_{40-55} are the most abundant. Some of them contain relics of high-Ca plagioclase ($An_{\geq 80}$) in the core. Crystals with patchy core An_{55-68}, thin Ca-rich intermediate zone An_{75-82} and oscillatory rim zones, and reversely zoned phenocrysts with Na-rich resorbed core An_{30-38} and Ca-rich patches An_{68-72} are less abundant but occur in all samples.

Orthopyroxenes (*Opx*) and clinopyroxenes (*Cpx*) (below 2 vol % in the lava dome rocks) form mainly subphenocrysts (100-300 μm) and microlites (<100 μm). *Opx* is represented by hypersthene $En_{69-76}Fs_{22-30}Wo_{1-4}$, and dominant *Cpx* composition corresponds to augite $Wo_{39-46}En_{42-45}Fs_{1-14}$. Weak reverse zoning of increasing Mg# from 0.68-0.70 in cores to 0.72-0.74 in rims was observed in *Opx* microlites from the most recently erupted andesites.

Andesites from 2001-2016 eruptions contain sporadic olivine (*Ol*) crystals ($Fo_{80–89}$) enclosed in reaction rim composed by *Opx*, Fe–Ti oxides, and *Amp* (Fig. 3d). Ti-magnetite and apatite are present in small amounts (~1 vol. %) in groundmass and as inclusions in phenocrysts. In samples of the 2001 eruption, rare anhydrite inclusions in *Pl* and *Amp* phenocrysts were reported by Humphreys et al. (2006). In andesites from the latest eruptive episodes, anhydrite inclusions occur in minor amounts within intergrowths of amphibole. Groundmass of the lava dome rocks typically consists of rhyolitic glass with microlites of plagioclase, subordinate pyroxene, amphibole, Ti-magnetite, and rare apatite.

5.2 Mafic enclaves

Mafic enclaves enriched in *Ol* and *Amp* phenocrysts were found in a lava block from the 2005 pyroclastic flow (Gorbach, Portnyagin, 2011). The enclaves are typically rounded, 5-7 cm in diameter and exhibit irregular embayed contact with host rock (Figs. 2d; 3e). The presence of up to 5 mm isometric pores, large olivine (0.5 - 1 mm) and abundant amphibole crystals are distinctive features of these enclaves among other types of inclusions and xenoliths, abundant in Shiveluch rocks (e.g., Melekestsev et al., 1991; Bryant et al., 2007). Pyroclastic deposits of 2010, 2013 and 2016 eruptions also contain enclaves of this type. A comprehensive petrological study of the mafic enclaves and cumulates hosted by the recently erupted Shiveluch andesites has been provided by Golu: et al. (2020).

Olivine phenocrysts range in composition from Fo_{92-88} in cores to Fo_{88-83} in rims and host inclusions of chromium spinel (molar Cr/(Cr+Al)×100=69-74; sample #7499-4 by Gorbach and Portnyagin, 2011). Acicular amphibole phenocrysts have distinctively high Al_2O_3 (~11-14 wt.%) content. Plagioclase phenocrysts occurs near the contact with the host andesite and exhibit signs of dissolution such as occurrence of sieved, enriched in melt inclusions zone between the crystal cores (An_{40-48}) and rims (An_{70-75}). This texture indicates incorporation of plagioclase from the host andesite into enclave, its reaction with melt inside enclave, and consequent crystallization (e.g., Humphreys et al., 2009b; Shcherbakov et al., 2011). Enclave matrix has a well-quenched texture (Fig. 3f) and consists of elongate *Pl* (An_{60-65}), *Amp* and *Cpx* microlites in a clear vesiculated glass.

5. 3 Major and trace elements

Andesites of the 1964 plinian and 1980-1981, 1993-1995 and 2001-2016 dome-forming eruptions contain from 60.5 to 64.0 wt.%. SiO_2 (Fig. 4a). The andesites have low-Fe (FeO*/MgO=1.09-1.39) and mid-K composition (K_2O=1.18-1.34 wt. %), high Mg# (Mg#=

0.56-0.62) and chromium contents (Cr ≥ 90-100 ppm), which are typical for Young Shiveluch rocks (e.g., Gorbach and Portnyagin, 2011; Ponomareva et al., 2007; 2015). Mafic enclaves are high-Mg# basaltic andesites (SiO_2=54.9-56.3 wt.%; K_2O=0.78-0.97 wt.% and Mg#=0.68-0.69).

SiO_2 contents in 1964, 1980-1981 and 1993-1995 andesites are within a narrow range of 60-62 wt.%, whereas 2001-2016 dome samples and pumice fragments from pyroclastic flows exhibit more variable compositions with SiO_2 ranging from 60 to 64 wt. %. The 2004-2005 dome rocks show the most silicic composition, while andesites of the following eruptions tend to slightly decrease in silica contents with time (Fig. 4b).

Trace elements patterns (Fig. 5a) for 1964 plinian, recently erupted Shiveluch andesite and mafic enclaves are typical for arc volcanoes. The rocks are enriched in LILE (K, Cs, U, Ba, Rb, Sr), Pb, LREE (La, Ce, Nd) and depleted in HFSE (Nb, Ta, Hf, Zr) and HREE (Tb, Dy, Ho, Er, Tm, Yb, Lu) compared to N-MORB. Chondrite-normalized REE contents exhibit strongly fractionated MREE (Sm, Eu, Gd), and unfractionated or slightly spoon-shaped HREE pattern similar in all rock varieties (Fig. 5b). Concentrations of HREE and Y are negatively correlated with silica content in andesites of the recent eruptions as well as in other Young Shiveluch rocks (Gorbach, Portnyagin, 2011).

5.4. Melt inclusions and matrix glasses

According to previously published data (Tolstykh et al., 1998; 2003; Humphreys et al., 2008) melt inclusions trapped by minerals in andesites of 1964 plinian and 1993 and 2001 dome-forming eruptions have rhyolite compositions with SiO_2≥69 wt.% (Fig. 4a). It is not excluded that some minerals in Shiveluch rocks crystallized from less evolved melts, which are compositionally closer to the host andesites, but there is presently no direct evidence for this from the melt inclusion record. Matrix glasses have more Si-rich compositions than melt inclusions and vary not systematically over time (Figs. 4a, 4b).

6. Amphibole occurrence, texture and chemistry

Amphiboles from Shiveluch andesites form mainly euhedral or sub-euhedral brown or reddish-brown phenocrysts with a predominant size from 0.5 to 2 mm (Figs. 3 a-b, 6 a-b). Opacitized amphiboles (Figs. 3c, 6c) occur in the samples of the early episode of the dome growth (1980-1981 and 1993-1995), sometimes in the contact zone of mafic enclaves with host rock and very rarely in 2001-2016 andesites. Amphiboles from mafic enclaves (thereafter referred to as "mafic" amphiboles) have typically an acicular shape (Figs. 3f, 6d). Anhedral amphiboles with embayed corroded margins (Fig. 6e) are abundant in the andesites from the latest eruptive episodes in 2013 and 2016. Amphibole subphenocrysts, microlites and cloths of crystals (Fig. 6e) were found in some andesites erupted in 2007, 2013 and 2016. Representative amphibole compositions for different Shiveluch eruptive events are given in Table 2. The full compositional data set and structural formula calculations according to the IMA2012 classification (Hawthorne et al., 2012) calculated using the AMFORM spreadsheet of Ridolfi et al. (2018) and also nomenclature according to Leake et al. (1997) is available in Supplementary Table B2. In the following text, we use the amphibole names after Leake et al. (1997) for simplicity and easy comparison with previously published data.

All Shiveluch amphiboles are calcic and contain $^{B}Ca>1.5$ apfu (atoms per formula unit) (Figs. 6g, 6h), and most of them are classified as magnesiohornblende (*Mhb*), pargasite (*Prg*) and magnesiohastingsite (*Mhs*). Subordinate number of the analysed amphiboles are tschermakite and edenite hornblendes (Figs. 6g, 6h).

Mhb predominate in the 1964 pumice and dome andesites and appear as middle-sized (≤1-1.2 mm, Fig. 6a) and large (≥1.5-2 mm, rarely up to 4-5 mm) phenocrysts (Fig. 6b). The *Mhb* often has heterogeneous cores with relics or patchy zones of *Prg* amphibole. Abundant inclusions of melt, plagioclase, orthopyroxene, apatite and Ti-magnetite are typical for such crystals, and the inclusions are often located concentrically around heterogeneous cores (Fig.

6b). "Mafic" amphiboles from enclaves are mainly *Mhs* and usually do not contain inclusions. In the contact zone between host andesite and enclaves, crystals of *Mhb* often have rims corresponding to *Mhs* composition (Fig. 6d). Anhedral resorbed crystals from the latest eruptive episode in 2013 and 2016 have patchy texture formed by *Mhb* and *Prg* in their cores (Fig. 6e).

The Shiveluch amphiboles exhibit a very wide range of chemical compositions (e.g., SiO_2=40.40-48.44 wt.%, TiO_2=0.36-3.45 wt.%, Al_2O_3=6.99-14.06 wt.%, FeO*=7.91-16.42 wt.%, MgO=11.61-17.44 wt.%, Na_2O=1.13-3.65 wt.% , K_2O=0.17-0.74 wt.%). The high-Al_2O_3 array of *Mhs* includes amphiboles from mafic enclaves and some amphiboles from the 1964, 2013 and 2016 eruptions (Fig. 7a). *Mhb* and *Prg* amphiboles are typical for most andesites. Besides high Al_2O_3 content, the "mafic" *Mhs* amphiboles have distinctively low Cl content (≤ 0.04 wt. %) in comparison with "andesitic" *Mhb* and *Prg* amphiboles (≥0.04 wt. %) (Fig. 7b).

The amphiboles display well expressed pressure-sensitive Al-Tschermak-type ($2Si^{IV}+Mg^{VI}=2Al^{IV}+Al^{VI}$) exchange and temperature-depended edenite-type ($Si^{IV}+()^{A}=Al^{IV}+(Na+K)^{A}$ exchange (Figs. 7c, 7d). Amphiboles from the dome rocks form continuous trend over the full range of Al^{IV} contents, whereas amphiboles from the 1964 pumice belong to two groups representing end members of the entire array. Ti-Tschermak-type temperature-depended exchange ($2Si^{IV} + Mn^{VI} = 2Al^{IV} + Ti^{VI}$) is weakly expressed in most of crystals from the lava dome andesite (Fig. 7e). A group of amphiboles with uncorrelated Ti and Al^{IV} is also present. This group includes some "mafic" amphiboles from enclaves and from the 1964 pumice. The plagioclase-type exchange ($Si^{IV} + Na^{A} = Al^{IV} + Ca^{A}$) is not evident for *Mhb* amphiboles (Al^{IV}<1.5 p.f.u.), whereas slight positive correlation is observed for *Mhs* and *Prg* amphiboles (Fig. 7f).

7. Amphibole zoning patterns

Representative examples of compositionally zoned amphibole crystals from different Shiveluch eruptions are illustrated in Figs. 8 and 9. Most of zoned crystals have either patchy core with irregular core-rim boundary (Fig. 8a) or homogeneous core surrounded by compositionally contrasting outer margin of variable thickness (Fig. 8b). Crystals with oscillatory zoning are rare. Complexly zoned grains containing patchy cores, compositionally contrasting intermediate zones and rims were mostly found in andesites of the latest eruptive episodes in 2013 and 2016.

Based on the chemical and textural data and considering cations substitutions, we distinguish simple (or normal), patchy and two types of reverse zoning in the amphiboles from the modern episode of the Shiveluch activity. The zoning patterns are expressed at best in the variations of Al_2O_3 and MgO as well as Mg#, Al^{IV}, Al^{VI} and $(Na+K)^A$, which are sensitive to variations in pressure, temperature and melt composition (e.g., Spear, 1981; Blundy & Holland, 1990, Johnson & Rutherford, 1989; Schmidt, 1992).

Amphiboles from the 1964 pumice are represented by two main types: phenocrysts with patchy cores and wide unzoned outer margins of different composition (Fig. 8a) and subphenocrysts with homogeneous core and narrow (10-20 μm) compositionally contrasting rim (Fig. 8b). Phenocrysts and subphenocrysts in 1964 andesites have similar composition. The patchy cores of phenocrysts (Fig. 8a, Table 2, #1) and the cores of subphenocrysts (Fig. 8b, Table 2, #3) correspond to *Mhs* and are characterized by low-Si (SiO_2~42-44 wt.%), high-Al (Al_2O_3~11-13 wt.%), relatively low-MgO (12-14 wt. %) and high $(Na+K)^A$ values. The outer margins of phenocrysts and subphenocrysts correspond to *Mhb*, in which Al_2O_3 (and also Al^{IV}, Al^{VI}) and $(Na+K)^A$ concentrations decrease drastically, whereas SiO_2, MgO, and Mg# sharply increase toward the crystal faces (Table 2, # 2 and #4). The decreasing abundances of a pressure-sensitive Al-Tschermak (Al^{IV} and Al^{VI}) and a temperature-controlled edenite ($(Na+K)^A$) end-members toward the rims of the studied crystals from the 1964 eruption correspond to simple (normal) zoning.

Amphibole phenocrysts from andesites erupted in 1980-1981 and 1993 are predominantly unzoned or weakly zoned low-Al (Al_2O_3~7-10.5 wt. %) *Mhb*. They are often surrounded by 70-100 μm-wide breakdown rims consisting of fine grained aggregate of *Cpx*, *Pl* and Fe-Ti oxides (Fig. 8c). Minor fluctuations of Al_2O_3 content are observed in phenocrysts that contain abundant inclusions of *Pl*, *Opx*, *Mt* and *Ap* (Fig. 8c).

Amphiboles from 2001 andesites have been described in detail by Humphreys et al. (2006). Similarly to the early dome-forming episode, unzoned low-Al *Mhb* are the most common but some crystals exhibit simple (normal) chemical zoning. In these normally zoned crystals, Al_2O_3 decreases from core (~9-9.5 wt%; Table 4 from Humphreys et al. 2006) to rim, and Mg, Na and Si contents increase. Patchy crystals have irregular partially resorbed high-Al cores and Al-poor rims. Crystals with complex zoning have an intermediate zone between core and rim, which is enriched in Mg and depleted in Al.

Amphiboles from mafic enclaves in 2005 andesites have high-Al (Al_2O_3~11-14 wt. %) and high-Mg# (up to 0.83) *Mhs* composition (Goltz et al., 2020). Typically, they have unzoned cores (Fig. 9a) mantled by thin rims, in which Al and Mg# slightly decrease. By contrast to normally zoned crystals in the mafic enclaves, amphiboles phenocrysts from the host andesite on the contact zone with the enclaves exhibit sharp reverse distribution of Al, Mg#, and $(Na+K)^A$ toward the rims (Fig. 9b). We define such pattern as reverse zoning of type 1. The cores of the reversely zoned crystals are low-Al *Mhb*, whereas rims correspond to *Mhs* (Table 2, #21-24). Al and $(Na+K)^A$ contents increase almost two times in the rims of such crystals (Fig. 9b) and correlate inversely with Si and Mg, decreasing sharply from core to rim.

Amphiboles from andesites of the latest eruptive episodes in 2013 and 2016 are the most heterogeneous with respect to the texture, composition and zoning. Similarly to previous eruptive episodes, crystals with high-Al patchy cores (e.g., Fig. 6b, # 27-28 in Table 2) are characterized by decreasing Al and $(Na+K)^A$ values and mirror changes of MgO and Mg#

toward the rims. Amphiboles from crystal cloths exhibit simple zoning for Al, $(Na+K)^A$ and Mg (Fig. 6e, # 33-34 in Table 2). Some amphiboles such as those with corroded margin or with low-Al cores are surrounded by rims enriched in Al, Mg and Mg# and depleted in Si (Fig. 9c, Table 2, #29-30). This distinctive zoning of amphiboles from the latest eruptive episode is further referred to as the reverse zoning of type 2.

8. Conditions of amphibole crystallization

8.1. Pressure and temperature

Empirical equations based on the results of equilibrium experiments with natural volcanic rocks at high *P-T* conditions have been proposed to quantitatively estimate the crystallization conditions of calcic amphiboles (Ridolfi et al., 2010; Ridolfi and Renzulli, 2012; Putirka, 2016). Compositionally homogeneous amphibole crystals or their parts, indicating crystallization at the condition of chemical equilibrium, are required to obtain reliable results from the amphibole-based thermobarometry (Ridolfi et al., 2016). The algorithm to distinguish suitable part of amphibole crystal for thermobarometric calculations has been recently proposed by Gorini et al (2018). According to this algorithm, amphiboles (or their zones) showing intra-crystalline compositional variability not exceeding typical variations of amphibole compositions from equilibrium experiments used to calibrate the thermobarometric equations of Ridolfi and Renzulli (2012), are considered as compositionally homogeneous and crystallized at equilibrium conditions (Gorini et al., 2018).

Application of the algorithm of Gorini et al. (2018) allowed us to identify the most suitable compositions for amphibole thermobarometry. The group of crystals of highly heterogeneous composition including reversely rimmed amphiboles from the contact zone of mafic enclaves with host andesites and some amphiboles with textures produced by fast growing from the andesites of the latest eruptive episodes were excluded from the thermobarometric calculations. Large compositional variations observed at the rims of these

crystals (Fig. 9b) reflect conditions of crystallization at strong chemical and thermal disequilibrium. The crystals from the inner part of mafic enclaves, the cores of subphenocrysts and the outer zones of phenocrysts from 1964 pumice, most of amphiboles from the 1993 eruption, and a part of amphiboles erupted in 2001-2016 satisfy the criteria of homogeneity by Gorini et al. (2018) and were used for thermobarometric calculations.

To estimate the crystallization temperature (*T*) for selected groups of crystals and their homogeneous zones, we used the pressure-independent equation of Putirka (2016) based on the largest dataset of experimental amphibole compositions. The estimates of crystallization pressure (*P*) were obtained using equations from a recent model of Ridolfi and Renzulli (2012) calibrated for the pressure range of 130-500 MPa. The thermobarometric equations and results of calculations are given in Supplementary Tables B2 and B3.

The *P-T* crystallization conditions calculated using amphibole-only calibrations (Eq. 5) of Putirka (2016) for *T*, and average *P* values from the equations 1b and 1c of Ridolfi and Renzulli (2012) are shown on Fig. 10a. The estimated range of the *P-T* conditions for all Shiveluch amphiboles are 845-1015 °C and 110-500 MPa. The lower estimates (*T*= 845-893˚C and *P*≤200 MPa) are characteristic for the low-Al *Mhb* from the lava dome rocks. The highest estimates (*T*=914-1015˚C and *P*=400-500 MPa) were obtained for high-Al *Mhs* crystals from the mafic enclaves and also for the cores of subphenocrysts from 1964 pumice. For *Prg* amphiboles, which typically compose the central zones in individual crystals from the latest eruptive episodes in 2013-2016, intermediate values (*T*=900-940˚C and *P*≤300 MPa) were calculated.

The crystallization temperatures estimated using model by Putirka (2016) for different events in the Shiveluch eruptive sequence are plotted on Fig. 10b. The data for amphiboles from 1964 pumice exhibit remarkable bimodal distribution with two populations corresponding to cores of subphenocrysts (930±20 ˚C, here and thereafter uncertainty corresponds to 2σ) and outer zones of phenoctysts and rims of subphenocrysts (858±14 ˚C).

Mainly unzoned crystals from andesites of the early episodes of the lava dome growth in 1993-1995 yielded 881±15 ˚C. The average *T* for cores of "mafic" amphiboles is 981±40 ˚C. A significant temperature range (from 861 to 924 ˚C) was obtained for amphibole cores from andesites erupted in 2001-2016.

To verify the calculation by the amphibole-only geothermometers (Putirka, 2016; Ridolfi and Renzulli, 2012) we compared our results with the estimates obtained using hornblende–plagioclase and Fe–Ti oxide thermometry reported in the previous works (Dirksen et al., 2006; Humphreys et al. 2006). In addition, we applied the equations of Simakin and Shaposnikova (2017) experimentally calibrated for *Mhs* amphibole from the Karan lava domes.

The temperatures calculated using model of Putirka (2016) (e.g., 2001-2004 eruptive events in Fig. 10b) are similar to the temperature range from 834°C to 978°C (on average 878°C) obtained by Humphreys et al. (2006) for 2001 andesites using Fe-Ti oxide pairs composition. In comparison with the results of hornblende–plagioclase thermometry (Holland, Blundy, 1994), the model of Putirka (2016) yields close, but slightly higher average values. For low-Al *Mhb* associated with *Pl* An_{40-55}, previous works reported temperatures of 840-860°C (e.g., Dirksen et al., 2006; Humphreys et al., 2006; Gorbach et al., 2016). The average temperature using Putirka (2016) for this mineral assemblage is 871±22°C (n=120). The difference in the average values, however, does not exceeds the uncertainties of these models, which correspond to ±40°C for Holland and Blundy (1994) model and ±30 °C for Putirka (2016) model.

The barometric data for low-Al *Mhb* ($P \leq 200$ MPa, on average 150±48 MPa) calculated using the model by Ridolfi and Renzulli (2012) are consistent with the maximum pressure ~160 MPa calculated based on H_2O content in melt inclusions and the dependence of its solubility on pressure (Tolstykh et al., 1998; 2003; Humphreys et al., 2006).

The barometric calculations performed using the method by Simakin and Shaposhnikova (2017) for "mafic" amphibole yielded the values 463-558 MPa, that are similar to the results using Ridolfi and Renzulli (2012) approach (Table 2). In addition, the compositions of amphiboles from the mafic enclaves are close to the amphibole compositions obtained during the experiments by Simakin and Shaposhnikova (2017) at a 500 MPa and 990°C (Fig. 10a). Therefore, high-Al amphibole crystals from the mafic enclaves and high-Al amphibole cores from the 1964 pumice could crystallize at *T*~940-1015 °C (on average 981±40 °C, n=36) and *P*~400-558 MPa.

8.2. Redox conditions and melt H_2O

Oxygen fugacity (fO_2) estimated using the model by Ridolfi et al. (2010) for *Mhb* population, that is the most common in the lava dome rocks, ranges from $10^{-9.7}$ to $10^{-12.0}$ atm (on average $10^{-11.2}$ atm) that corresponds to 1.0–2.1 log units of fO_2 above the nickel–nickel oxide oxygen buffer (NNO). These oxidizing conditions are similar to those estimated for 2001 andesites by Humphreys et al. (2006) from Fe–Ti oxide equilibria (ΔNNO~ 1.5-2.1). The fO_2 for *Mhs* crystals from mafic enclaves and high-Al cores from amphiboles of the 1964 plinian eruption gave ΔNNO ~ 0.2-1.6 log by model of Ridolfi et al. (2010).

The melt H_2O contents calculated using model by Ridolfi et al. (2010) for *Mhb* population vary from ~3.5 to 6 wt.%. The results are consistent with the data on H_2O content in melt inclusions in plagioclase and amphibole from the 1964 pumice, 1993 lava dome andesite and 2001 andesite, which range from 3.0 to 7.2 wt% (on average 4.7 wt. %) (Tolstykh et al. 1998; 2003; Humphreys et al., 2008). For the parental magma of "mafic" amphibole, Goltz et al. (2020) report very high H_2O content (>8 wt. %) based on the amphibole hygrometer of Krawczynski et al. (2012). Our estimation using approach by Ridolfi et al. (2010) yields similar values (~6.1-8.0 wt.%), which are higher in comparison with other primitive Kamchatka magmas (e.g., Portnyagin et al., 2007; Mironov et al., 2015;

Kamenetsky et al., 2018; Tobelko et al., 2020) and subduction-related magmas in general (e.g., Plank et al., 2013). Comparably high H_2O contents (~6.4 wt. %) were estimated by Gavrilenko et al. (2016) for parental melts of high-K_2O basaltic tephra erupted at Shiveluch volcano ~3900 BP (SHsp Unit#28, Ponomareva et al., 2015) in equilibrium with olivine $Fo_{92.5}$.

9. Discussion

9.1. Multiple amphibole populations in recently erupted Shiveluch andesites

There are many active andesitic and dacitic arc volcanoes, for example, Pinatubo (Pallister et al., 1996), Soufrie`re Hills (Murphy et al., 2000), Unsen (Sato et al., 2005), Mount Saint Helens (Thornber et al., 2008), Quizapu (Ruprecht et al., 2012), Augustine (De Angelis et al, 2013), Merapi (Erdman et al., 2014), whose volcanic products bear evidence of a large complexity of pre-eruptive magmatic processes, as reflected, among others features, by the presence of multiple amphibole populations.

Andesites of the ongoing Shiveluch eruption also belong to this list and exhibit a large compositional variability of amphiboles ranging from low-Al *Mhb* to high-Al *Mhs* and *Prg* on the scale of rock samples and within individual crystals (Figs. 6-9). In some cases, for example, at Augustine (De Angelis et al, 2013) and Merapi volcanoes (Erdman et al., 2014), the coexisting low- and high-Al amphiboles testify for mixing of mafic and silicic magmas at isobaric conditions and do not necessarily reflect crystallization over a large depth range. Alternatively, a similar amphibole systematics in volcanic rock can result from mixing of magma batches crystallized in at different depths (e.g., Thornber et al., 2008; Chambefort et al., 2013; Kent, 2014), or from mixing within a vertically extended magma reservoir or crystal mush column (e.g., Pichavant et al. 2002; Zhang et al., 2017; Humphreys et al., 2019).

Our thermobarometric results indicate that the diversity of amphibole compositions in Shiveluch andesites could originate from polybaric magma crystallization and magma mixing

processes, which begin in the mafic storage zone at the low-to-middle crustal depth and continued at shallow depths. The high-Al *Mhs* amphiboles could originate by crystallization of hydrous mafic high-*T* magma at great depth, whereas low-Al *Mhb* are sourced from low-*T* silicic magma in the shallow magma storage zone. The complexly zoned crystals with wide variation in Al content could be formed due to mixing and hybridization processes during the replenishment of shallow reservoir by mafic magma from depth. Below we summarize the evidence for this petrogenetic scenario obtained by analysis of amphibole composition.

9.1.1 The evidences of amphibole crystallization at lower-to-middle crystal depth beneath Shiveluch

The mineral assemblage of high-Al amphibole and *Fo*-rich olivine of the mafic enclaves sheds a light on the origin of deep magma feeding ongoing Shiveluch eruption. First of all, the presence of Fo-rich olivines with inclusions of chromium spinel implies that the enclaves crystallized from a high-Mg# primitive magma with high Cr and Ni contents. Secondly, olivine from the enclaves has similar composition to olivine from several other Holocene eruptions of Shiveluch volcano such as high-Mg# high-K basaltic tephra erupted ~3900 BP (Volynets et al., 1997), high-Mg# andesite lava of the early period of Young Shiveluch activity (samples ##7487, 7493; Gorbach, Portnyagin, 2011), and andesite from Karan domes (sample #7516-1; Gorbach, Portnyagin, 2011). The presence of high-*Fo* olivine associated with high-Al amphibole phenocrysts is a common feature of all these rocks as well as of mafic enclaves in recently erupted andesites.

The occurrence of the mineral assemblage of *Ol+CrSp ± Cpx ± Amp* observed in the mafic enclaves and some other Shiveluch rocks implies its derivation from a very H_2O-rich mafic magma at lower-to-middle crustal depths. Some experimental works suggested that such mineral assemblage could crystallize at pressures ≥500 MPa and $H_2O \geq 9$ wt.% in magma (Grove et al., 2003; 2005; Krawczynski et al., 2012). The recognition of amphibole

inclusions in high-*Fo* olivine in some enclaves is consistent with the super-hydrous (≥8 wt. % H_2O) composition of the Shiveluch parental magma, fractionating amphibole and olivine early on its liquid line of descent (Goltz et al., 2020). Our barometric calculations for *Mhs* amphibole from mafic enclaves suggest a pressure range of 400-558 MPa, which is close to the predictions from the experimental works, including high-pressure experiments with Shiveluch andesites (Simakin and Shaposhnikova, 2017). Assuming a crustal density of 2.7 g/cm^3, the pressure estimates correspond to the depths of 15-20 km beneath Shiveluch volcano. The recurrent occurrence of *Ol* and *Amp*-rich rock in the Shiveluch eruptive history can be considered as evidence in favor of the existence of a long-lived lower crustal magma storage zone beneath the volcano.

9.1.2. The shallow magma storage zone

The results of this study together with the previously published data (Tolstykh et al., 1998; 2003; Dirksen et al., 2006; Humphreys et al., 2006; 2008; Gorbach et al., 2016) demonstrate that the mineral association of *Mhb* and *Pl* An_{40-55} is the most common in Shiveluch andesites crystallized at 150 ± 48 MPa corresponding to the upper crustal depth of ~5-6 km. These data are consistent with the location of syn-eruptive earthquakes that are mostly restricted to depths of ≤5 km (Gorelchic et al., 1997; Senyukov et al., 2003) during Shiveluch lava dome growth episodes since 1980. Thus, both petrological and seismic data suggest the existence of a shallow, upper crustal magma reservoir beneath Shiveluch volcano at 5-6 km depth.

9.2. Interpretation of amphibole zoning

Simple (or normal) zoning of calcic amphiboles is typically characterized by Si increase and Al decrease from core to rim (e.g., Ridolfi et al., 2010; 2016; Gorini et al., 2018) and reflects crystallization from progressively evolving melt at decreasing *T* and *P*. The

normally zoned amphibole crystals are very typical in the 1964 Shiveluch pumice (Table 2, ##3-4). Their cores crystallized at T=914-946°C and P >400 MPa, outer zones of phenocrysts and rims of subphenocrysts – at T=845-869 °C and P= 112-142 MPa. The textural and size difference between phenocrysts with patchy cores and subphenocrysts with sharp compositional rim is most likely related to different ascent rates and residence time in the shallow magma chamber. The crystals with high-Al core and narrow Al-poor rims (Fig. 8b) could originate from a rapidly rising batch of magma, whereas crystals with patchy cores and wide outer zones (Fig. 8a) could crystallize from magma stalled at shallow depths for longer time.

Patchy zoning can form due to skeletal growth of crystals or due to resorption of previously formed crystals (e.g., Humphreys et al., 2006; Streck, 2008; Kiss et al., 2014). The process may be similar to that proposed for the origin of patchy plagioclase (Nelson & Montana, 1992). Most likely, both processes of skeletal growth and resorption were involved in the origin of the patchy zoned amphibole crystals in the Shiveluch rocks. The rapid decompression and resorption at shallow depths can readily explain the origin of the crystals with high-Al patchy cores surrounded by Al-poor rims. Al, $(Na+K)^A$, Mg, and Si distribution in these crystals is similar to that in crystals with simple zoning (Fig. 8a, b). Resorption due to mafic replenishment is more appropriate for patchy crystals with more complex Al, $(Na+K)^A$, Mg, and Si patterns such as in amphiboles from the latest Shiveluch eruptions.

Reverse zoning of calcic amphiboles is expressed in increasing Al and decreasing Si toward crystals rims as opposed to the simple (or normal) zoning (Gorini et al., 2018) reflects a process of amphibole crystallization at disequilibrium conditions caused by rapid changes of physicochemical parameters. The reverse rims distinguished in the studied amphiboles were most likely formed in response to replenishment of silicic magma with a batch of mafic magma.

Reversely zoned amphiboles of type 1 have rims enriched in Al and $(Na+K)^A$ and depleted in Si and Mg. The occurrence of these crystals in andesite close to contacts with mafic enclaves suggests that this zoning could be formed due reheating of the host andesite by mafic magma. In contrast, r*eversely zoned amphiboles of type 2* are characterized by the concomitant increase of Al and Mg in their rims (Fig. 9c). This type of zoning can result from mixing of mafic and silicic magmas, which leads to increasing Mg# and decreasing SiO_2 in the hybrid magma and to concomitantly increasing Mg# and Al content in the equilibrium amphibole (Sato et al., 2005; Kiss et al. 2014). Thus, the reversely zoned amphiboles of type 1 and 2, can represent different stages of interaction of mafic and silicic magmas. The type 1 crystals indicate reheating of silicic magma close to contact with mafic magma, whereas the type 2 crystals provide evidence for mixing of mafic and silicic magma and crystallization of amphibole from hybrid magma.

9.3. Shallow magmatic processes and eruptive dynamics

9.3.1. 1964 plinian eruption: influx of deeper magma as precondition

The latest plinian Shiveluch eruption occurred on November 11, 1964 following depressurization caused by the edifice failure and generation of giant debris avalanche (e.g., Belousov, 1995). According to our new data, an important role in triggering the eruption could play a mafic magma influx in the shallow magma chamber, which occurred shortly before the plinian eruption. The 10-20 μm-thin Al-poor rims of high-Al crystals in 1964 pumice record the rapid magma ascent from the lower crust to the shallow Shiveluch storage zone. (Fig. 11). The experimentally determined amphibole crystals growth rate (e.g., 5–10×10^{-8} cm/s; Simakin et al., 2009) suggest that such rims could be formed in a few hours. These data are consistent with the time of the strongest seismic events that occurred beneath Shiveluch 6 and 4 hours before the eruption (Zobin, 1971).

9.3.2. Slow and intermittent growth of lava dome in 1980-1981 and 1993-1995: cooling and crystallization in shallow magma chamber

In August 1980, sixteen years after 1964 eruption lava dome began to extrude. The absence of explosive and seismic precursors of the small-volume initial episode of the dome growth indicates a very slow magma ascent. The next pulse of the lava dome growth in 1993-1995 produced andesites with amphiboles exhibiting breakdown rims corresponding to decompression crystallization of a slowly rising magma. Amphiboles from the 1980-1981 and 1993-1995 episodes of the dome growth are mainly unzoned crystals of low-Al composition that indicates crystallization at T~881±15°C and P=150±48 MPa and corresponds to the conditions of a shallow magma chamber. The start of the magma ascent and dome growth could be induced by an overpressure caused by cooling, crystallization and degassing of magma (Sparks, 1997) in the upper part of the shallow magma chamber (Fig. 11).

9.3.3. Voluminous and persistent dome-building period in 2000s: mafic influx, mixing and hybridization

Both volcanological observations and petrological data suggest a recent influx of deep magma in the Shiveluch plumbing system in the early 2000s. Firstly, the increase of magma discharge rate in 2001-2016 could be considered as the response to overpressure in the shallow magma chamber due to the arrival of magma from depth (e.g., Eichelberger, 1995; Sparks, 1997). Secondly, the highly explosive activity in this period may reflect the processes of an exsolution of volatiles from the mafic magma during cooling and subsequent crystallization and/or a release of volatiles from the silicic magma during convection forced by mafic magma input (e.g., Folch, Marti, 1998).

Considerable macroscopic and microscopic evidence of magma mixing was firstly documented for 2001-2004 andesites (Humpherys et al., 2006; Dirksen et al., 2006; Gorbach, 2006). Based on the estimated residence time of olivine xenocrysts in silicic magma, Dirksen

et al. (2006) showed that the mafic magma replenishment occurred over timescales of 2 months to 4 years before the 2001 eruption.

The complexly zoned amphibole population in the andesites erupted in the 2000s (Fig. 11) records unstable conditions of frequent explosive and persistent extrusive recharge-driven eruptions. The absence of breakdown or reaction rims of amphibole crystals, close to skeletal form of crystals from rocks of the latest eruptive episodes correspond to high rates of magma ascent. The evidence of interaction between mafic and silicic magma was preserved in the zoned crystals from contacts of enclaves and host andesites. The sharply increasing Al and decreasing Mg# in the rims of amphiboles with reverse type 1 zoning is explained by the temperature impact of the enclave-forming magma on the host silicic melt. The rims with concomitant increase of Mg# and Al in reverse type 2 zoned crystals from the most recently erupted andesite is associated with amphibole growth following the mafic replenishment in the silicic magma storage zone. Some crystals in recently erupted Shiveluch andesites may originate from mafic magma due to disaggregation or erosion of the mafic enclaves (Humphreys et al., 2009b, Ruprecht et al., 2020). Correlated high Al content, low Cl and high Mg# may help to identify such crystals.

9.3.4 The sequence from 1964 plinian to ongoing dome-forming Shiveluch eruptions

Our interpretation of the amphibole chemistry and its zoning suggests that deep magma input in the shallow storage zone beneath Shiveluch occurred prior to the 1964 eruption and during the 2001-2016 period of extensive lava dome growth (Fig. 11). Since the 1964 plinian eruption was directly provoked by the decompression in magma reservoir following the collapse of volcanic edifice (Belousov, 1995), the arrival of deeper magma at the shallow crustal level can be considered as an important precondition for this catastrophic eruption. For the 2001-2016 dome-forming period, the mafic magma influx was syn-eruptive

and, probably, hotter and more voluminous compared to 1964 eruption. These eruptive sequences are consistent with the model of Ruprecht and Bachmann (2010) based on the volume of mafic recharge and its thermal and viscosity effects on the efficiency of magma mixing. Volumetrically significant mafic recharge provides sufficient reheating by thorough mixing between silicic and mafic magmas and suppresses the defragmentation process that leads to effusive (dome-forming) eruption. In contrast, minor influx of deeper magma does not cause reheating significant volume of silicic magma, but leads to increasing of magma overpressure and favors explosive eruption (Ruprecht and Bachmann, 2010).

10. Conclusions

1) Amphibole crystals from andesites of the 1964 plinian eruptions and the following dome-building eruptions at Shiveluch volcano are compositionally diverse and range from low-Al *Mhb* to high-Al *Mhs* and *Prg* in different rock samples and on the scale of single crystals. Compositional and textural diversity of the amphibole compositions from the andesites and associated mafic enclaves implies that both magma mixing process and variable *P-T* conditions affected amphibole crystallization.

2) The high-Al *Mhs* amphiboles originate by crystallization of hydrous mafic high-temperature magma at great depth, whereas low-Al *Mhb* are sourced from the lower-temperature silicic magma in the shallow magma storage zone. The complexly zoned crystals with a wide variation in Al content were formed due to mixing processes during the replenishment of shallow reservoir by deeper magma.

3) Amphibole-based barometric calculations obtained by different approaches and comparison with experimental data yielded consistent results and suggested that Shiveluch plumbing systems consist of the mafic and silicic storage zones in the mid-to-lower crust (~ 15-20 km depth) and in the upper crust (~ 5-6 km depth), respectively.

4) Simple (normal), patchy, and two types of reverse zoning were distinguished in the Shiveluch amphiboles based on their chemical composition and textural patterns. The discontinuous compositional rims of normally zoned high-Al crystal from 1964 plinian pumice recorded a rapid depressurization and magma ascent from the deep mafic to the shallow silicic magma chamber. Mainly unzoned *Mhb* crystals from the early Shiveluch dome-building episodes in 1993-1995 suggest magma cooling and crystallization in the shallow magma chamber. Complexly zoned amphiboles from andesites erupted in the 2000s reflect periodic mafic magma replenishments and syn-eruptive mixing mafic and silicic magmas.

5) We present a schematic model combining the new data on the shallow magmatic processes and eruptive dynamics for the Shiveluch 1964 plinian and the following dome-forming eruptions. The model suggests that the influx of deeper magma from the lower crust to the shallow silicic storage zone beneath the volcano occurred before the 1964 plinian eruption and also during the period of extensive lava dome growth in 2001-2016. The different styles of the recent Shiveluch eruptions may be controlled by the relative volume of the mafic recharges and their thermal and viscosity effects on the efficiency of magma mixing.

The following are the supplementary data related to this article.

Table B1. Major and trace element composition of recent Shiveluch rocks

Table B2. Shiveluch amphibole composition and intensive parameters calculation

Table B3. Thermobarometric and chemometric equations used in this study

Acknowledgments

We are very grateful to Raya Sagitova, Igor Tembrel and Alexander Nozhikov for invaluable help during the Shiveluch field works. We are thankful to Yuri Dubic, Alexander and Marina Belousov's and Sergey Khubunaya for providing samples of 1980, 1993 and 2001 Shiveluch eruptions. Dieter Garbe-Schönberg and Ulrike Westernstroer are thanked for

performing ICP-MS analyses at Kiel University. We are grateful Mario Thöner for his assistance with EPMA studies in GEOMAR. This work was supported by grants #15-05-06440_a from the Russian Foundation for Basic Research (N.G. and T.P.) and grant #16-17-10035 from the Russian Science Foundation (M.P.). We acknowledge GEOMAR (Kiel, Germany) funding for the electron microprobe, part of XRF and ICP-MS analyses. We are very thankful to Phillip Ruprecht and an anonymous reviewer for their helpful suggestions on how to improve our manuscript.

CRediT author statement

Natalia Gorbach: Conceptualization, Field works, Investigation, Formal analysis, Writing - Original Draft;
Tatiana Philosofova: Resources, Software, Investigation;
Maxim Portnyagin: Resources, Data Curation, Validation, Writing - Review & Editing.

Declaration of interests

The authors declare that they have no known competing financial interests or personal relationships that could have appeared to influence the work reported in this paper.

References

Anderson, J. L., Smith, D.R., 1995. The effects of temperature and fO2 on the Al-in-hornblende barometer. American Mineralogist. 80: 549–559.

Almeev, R. R., Arislan, A. A., Ozerov, A.Y., Kononkova, N.N., 2002. Problems of the stoichiometry and thermobarometry of magmatic amphiboles: an example of hornblende from the andesites of Bezymianny volcano, Eastern Kamchatka. Geochemistry International. 40 (8): 723–738.

Auer, A., Belousov, A., Belousova, M., 2018. Deposits, petrology and mechanism of the 2010–2013 eruption of Kizimen volcano in Kamchatka, Russia. Bulletin of Volcanology, 80(4): 33. doi.org/10.1007/s00445-018-1199-z

Belousov, A. B., 1995. The Shiveluch volcanic eruption of 12 November 1964—explosive eruption provoked by failure of the edifice. Journal of Volcanology and Geothermal Research. 66: 357–365.

Blundy, J., Holland, T.J.B., 1990. Calcic amphibole equilibria and a new amphibole-plagioclase geothermometer. Contribution to Mineralogy and Petrology. 204: 208-224.

Cassidy, M., Manga, M., Cashman, K., & Bachmann, O., 2018. Controls on explosive-effusive volcanic eruption styles. Nature Communications, 9(1): 1-16. DOI: 10.1038/s41467-018-05293-3

Chambefort I., Dilles J. H., Longo A., 2013. Amphibole Geochemistry of the Yanacocha Volcanics, Peru: Evidence for Diverse Sources of Magmatic Volatiles Related to Gold Ores. Journal of Petrology. 54, (5):1017-1046. doi.org/10.1093/petrology/egt004

Churikova T.G., Ivanov B. V., Eichelberger J., Worner G., Browne B., and Izbekov P., 2013. Major and Trace Element Zoning in Plagioclase from Kizimen Volcano (Kamchatka): Insights into Magma Chamber Processes. Journal of Volcanology and Seismology. 7(2):112-130. doi.org/10.1134/S0742046313020024

De Angelis, S. H., Larsen, J., & Coombs, M., 2013. Pre-eruptive magmatic conditions at Augustine Volcano, Alaska, 2006: evidence from amphibole geochemistry and textures. Journal of Petrology. 54, (9): 1939-1961. doi.org/10.1093/petrology/egt037

Dirksen, O., Humphreys, M. C. S., Pletchov, P. et al., 2006. The 2001–2004 dome-forming eruption of Shiveluch volcano, Kamchatka: Observation, petrological investigation and numerical modelling. Journal of volcanology and geothermal research. 155 (3): 201-226. doi.org/10.1016/j.jvolgeores.2006.03.029

Dvigalo, V. N., 1984. Growth of the dome in the crater of Shiveluch volcano in 1980-1981 according to photogrammetric data. Vulkanol. Seismol. 2: 104-109 (In Russian).

Ivanov, B.V., Chirkov, A.M., Dubik, Yu.M., et al., 1981. The state of volcanoes in Kamchatka and the Kuril Islands in 1980. Vulkanol. Seismol., 3: 99–104 (In Russian).

Ivanov, B.V., 2008. Andesites of Kamchatka: Chemical Analyses of Volcanic Rocks and Major Rock Forming Minerals, Moscow: Nauka.

Izbekov, P. E., Eichelberger, J. C., Patino, L. C., & Vogel, T. A., 2002. Calcific cores of plagioclase phenocrysts in andesite from Karymsky volcano: Evidence for rapid introduction by basaltic replenishment. Geology, 30(9): 799-8.

Erdmann, S., Martel, C., Pichavant, M., & Kushnir, A., 2014. Amphibole as an archivist of magmatic crystallization conditions: problems, potential, and implications for inferring magma storage prior to the paroxysmal 2010 eruption of Mount Merapi, Indonesia. Contributions to Mineralogy and Petrology. 167, (6): 1016. doi.org/10.1007/s00410-014-1016-4

Eichelberger, J. C.,1980. Vesiculation of mafic magmas during replenishment of silicic magma reservoirs. Nature. 288: 446–450.

Eichelberger, J. C.,1995. Silicic volcanism: ascent of viscous magmas from crustal reservoirs. Annual Review of Earth and Planetary Science. 23: 41–63.

Fedotov, S. A., Dvigalo, V. N., & Zharinov, N. A., 2001. The May–July 2001 Eruption of Shiveluch Volcano. Vulkanol. Seismol. (6): 1-13. (In Russian).

Folch A, Marti J., 1998. The generation of overpressure in felsic magma chambers by replenishment. Earth and Planetary Science Letters. 163, (1): 301-314.

Gavrilenko, M., Herzberg, C., Vidito, C., Carr, M. J., Tenner, T., & Ozerov, A., 2016. A calcium-in-olivine geohygrometer and its application to subduction zone magmatism. Journal of Petrology. 57(9): 1811-1832. doi.org/10.1093/petrology/egw062

Garbe-Schönberg, D., 1993. Simultaneous determination of 37 trace elements in 28 international rock standards by ICP-MS. Geostandards Newsletter, 17: 81-93.

Ginibre C., Wörner G., Kronz A., 2007. Crystal zoning as an archive for magma evolution. Elements. 3 (4): 261–266.

Girina, O.A., Nuzhdaev, A.A., 2014. On some features peculiar to the September 22, 2005 eruption of Molodoi Shiveluch Volcano, Kamchatka. Journal of Volcanology and Seismology. 8, (4): 218–227.

Goltz, A., Krawczynski, M. J., Gavrilenko, M., Gorbach N. & Ruprecht, P., 2020. Evidence for Superhydrous Primitive Arc Magmas from Mafic Enclaves at Shiveluch Volcano, Kamchatka. Contributions to Mineralogy and Petrology, under review.

Gorbach, N. V. 2006. The first lava flow on the extrusive dome of Shiveluch volcano, 2004. Journal of Volcanology and Seismology. 2: 9-16. (in Russian).

Gorbach N. V., Portnyagin, M. V., 2011. Geology and petrology of the lava complex of Young Shiveluch Volcano, Kamchatka. Petrology. 19, (2): 134-166. https://doi.org/10.1134/S0869591111020068

Gorbach, N., Portnyagin, M., & Tembrel, I., 2013. Volcanic structure and composition of Old Shiveluch volcano, Kamchatka. Journal of Volcanology and Geothermal research. 263: 193-208. doi: 10.1016/j.jvolgeores.2012.12.012.

Gorbach, N. V., Portnyagin, M. V., & Philosofova, T. M., 2016. Dynamics of exrtrusive dome growth and variations in chemical and mineralogical composition of Young Shiveluch andesites in 2001–2013. Journal of Volcanology and Seismology. 10, (6): 360-381. https://doi.org/10.1134/S0742046316060038

Gorelchik, V.I., Shirokov, V.A., Firstov P.P., Chubarova O.S., 1997. Shiveluch volcano: seismicity, deep structure and forecasting eruptions (Kamchatka). Journal of Volcanology and Geothermal Research. 78, (1–2): 121 - 137. doi: 10.1016/S0377-0273(96)00108-4.

Gorini, A., Ridolfi, F., Piscaglia, F., Taussi, M. and Renzulli, A., 2018. Application and reliability of calcic amphibole thermobarometry as inferred from calc-alkaline products of active geothermal areas in the Andes. Journal of Volcanology and Geothermal Research, 358; 58-76. https://doi.org/10.1016/j.jvolgeores.2018.03.018

Gorshkov, G. S., Dubik, Yu. M., 1970. Gigantic directed blast at Shiveluch volcano (Kamchatka). Bulletin of Volcanology. 34: 261-288.

Grove, T. L., Elkins-Tanton, L. T., Parman, S. W., Chatterjee, N., Müntener, O., & Gaetani, G. A., 2003. Fractional crystallization and mantle-melting controls on calc-alkaline differentiation trends. Contributions to Mineralogy and Petrology, 145, (5): 515-533.

Hawthorne, F.C., Oberti, R., Harlow, G.E., Maresch, W.V., Martin, R.F., Schumacher, J.C., Welch, M.D., 2012. IMA report Nomenclature of the amphibole supergroup. Am. Mineral. 97, 2031-2048.

Holland, T. and Blundy, J. D., 1994. Non-ideal interactions in calcic amphiboles and their bearing on amphibole–plagioclase thermometry. Contributions to Mineralogy and Petrology. 116: 433–447.

Humphreys, M. C. S., Blundy, J. D., Sparks, R.S.J., 2006. Magma Evolution and Open-System Processes at Shiveluch Volcano: Insights from Phenocryst Zoning. Journal of Petrology. 47, (12): 2303-2334. https://doi.org/10.1093/petrology/egl045

Humphreys, M. C. S., Blundy J. D., Sparks R.S.J., 2008. Shallow-level decompression crystallisation and deep magma supply at Shiveluch Volcano. Contributions to Mineralogy and Petrology. 155: 45-61. https://doi.org/10.1007/s00410-007-0223-7

Humphreys, M. C. S., Edmonds, M., Christopher, T., & Hards, V., 2009a. Chlorine variations in the magma of Soufrière Hills Volcano, Montserrat: Insights from Cl in hornblende and melt inclusions. Geochimica et Cosmochimica Acta, 73, (19): 5693-5708. https://doi.org/10.1016/j.gca.2009.06.014

Humphreys, M. C., Christopher, T., & Hards, V., 2009b. Microlite transfer by disaggregation of mafic inclusions following magma mixing at Soufrière Hills volcano, Montserrat. Contributions to Mineralogy and Petrology, 157,(5): 609-624. https://doi.org/10.1007/s00410-008-0356-3

Humphreys, M. C., Cooper, G. F., Zhang, J., Loewen, M., Kent, A. J., Macpherson, C. G., & Davidson, J. P., 2019. Unravelling the complexity of magma plumbing at Mount St. Helens: a new trace element partitioning scheme for amphibole. Contributions to Mineralogy and Petrology, 174(1): 9.

Jarosewich, E., Nelen J. A., Norberg J. A., 1980. Reference Samples for Electron Microprobe Analysis. Geostand. Newslett. 4: 43-47.

Johnson, M.C., Rutherford, M. J., 1989. Experimental calibration of the aluminum-in-hornblende geobarometer with application to Long Valley caldera (California) volcanic rocks Geology. 17, (9): 837–841.

Jochum, K., P., Nohl, U., Herwig, K., Lammel, E., Stoll, B., Hofmann., A. W., 2005 GeoReM: A New Geochemical Database for Reference Materials and Isotopic Standards. Geostandards and Geoanalytical Research, 29 (3): 333-338. 10.1111/j.1751-908X.2005.tb00904.x

Kamenetsky, V.S., Zelenski, M., Gurenko, A., Portnyagin, M., Ehrig, K., Kamenetsky, M., Churikova, T., Feig, S., 2017. Silicate-sulfide liquid immiscibility in modern arc basalt (Tolbachik volcano, Kamchatka): Part II. Composition, liquidus assemblage and fractionation of the silicate melt. Chemical Geology 471, 92-110, https://doi.org/110.1016/j.chemgeo.2017.1009.1019.

Kiss, B., Harangi, S., Ntaflos, T. et al., 2014. Amphibole perspective to unravel pre-eruptive processes and conditions in volcanic plumbing systems beneath intermediate arc volcanoes: a case study from Ciomadul volcano (SE Carpathians). Contributions to Mineralogy and Petrology, 167(3): 986. https://doi.org/10.1007/s00410-014-0986-6

Khubunaya, S. A., Zharinov, N. A., Muravyev, Ya. D, et al. 1995. 1993 eruption of Shiveluch volcano. Volcanol Seismol. 17: 1-20 (in Russian).

Krawczynski, M. J., Grove, T. L. & Behrens, H., 2012. Amphibole stability in primitive arc magmas: effects of temperature, H_2O content, and oxygen fugacity. Contributions to Mineralogy and Petrology. 164: 317-339. https://doi.org/10.1007/s00410-012-0740-x

Krippner, J.B., Belousov, A.B., Belousova, M.G., Ramsey, M.S., 2018. Parametric analysis of lava dome-collapse events and pyroclastic deposits at Shiveluch volcano, Kamchatka, using visible and infrared satellite data. Journal of Volcanology and Geothermal Research. 354: 115-129. https://doi.org/10.1016/j.jvolgeores.2018.01.027

Kyle, P.R., Ponomareva, V. V., Rourke Schluep, R., 2011. Geochemical characterization of marker tephra layers from major Holocene eruptions, Kamchatka Peninsula, Russia. Int. Geol. Rev. 53, 1059–1097. https://doi.org/10.1080/00206810903442162

Leake B.E., Woolley A.R., Arps C.E.S. et al., 1997. Nomenclature of amphiboles: Report of the Subcommittee on Amphiboles of the Mineralogical Association. Mineralogical Magazine. 61 (3): 295 – 321.

Melekestsev, I. V., Volynets, O. N., Ermakov, V. A., et al., 1991. Shiveluch volcano. In: Fedotov SA, Masurenkov YuP (eds) Active volcanoes of Kamchatka, Vol 1. Nauka Press, Moscow: 84-103.

Melekestsev, I.V., Dvigalo, V.N., Kirsanova, T.P., et al., 2004. The 300 years of the life of Kamchatkan volcanoes: Molodoi Shiveluch (an analysis of the dynamics and impact of its eruptive activity during the 17–20th centuries). Part I. 1650–1964. Vulkanol. Seismol. 1: 3–19. (in Russian).

Menyailov, A.A., 1955. Shiveluch Volcano, its geologic structure, composition and eruptions. Trudi Laboratorii Vulkanologii, 9. (in Russian).

Mironov, N., Portnyagin, M., Botcharnikov, R., Gurenko, A., Hoernle, K., Holtz, F., 2015. Quantification of the CO2 budget and H2O–CO2 systematics in subduction-zone magmas through the experimental hydration of melt inclusions in olivine at high H2O pressure. Earth Planet. Sci. Lett. 425, 1-11. https://doi.org/10.1016/j.epsl.2015.05.043

Murphy, M. D., Sparks R. S. J., Barclay J. et al., 2000. Remobilization of Andesite Magma by Intrusion of Mafic Magma at the Soufriere Hills Volcano, Montserrat, West Indies. Journal of Petrology. 41 (1): 21–42.

Ovsyannikov, A. A., Manevich, A.G., 2010. Eruption of Shiveluch volcano in October 2010. Bulletin of Kamchatka Association "Educational-Scientific Center" 16(2): 7-9. (In Russian).

Pallister, J. S., Hoblitt, R.P., Meeker, G.P. et al., 1996. Magma mixing at Mount Pinatubo: petrographic and chemical evidence from the 1991 deposits. In: Newhall CG, Punongbayan RS (eds) Fire and Mud: Eruptions and Lahars of Mount Pinatubo, Philippines. University of Washington Press. Seattle: 687–731.

Pevzner, M.M., Tolstykh, M.L., Babansky, A.D., Kononkova, N.N., 2013. Reconstruction of the magmatic system in the Shiveluch volcanic massif as a result of large-scale collapses of its edifice in the late Pleistocene-early Holocene. Doklady Earth Sciences. 448 (1): 35-37. https://doi.org/10.1134/S1028334X1210011X

Piip, B. I., & Markhinin, E. K., 1965. Gigantic eruption of Shiveluch Volcano on November 12, 1964. Bull. vulk. st. AN SSSR. (39).

Plank, T., Kelley, K.A., Zimmer, M.M., Hauri, E.H., Wallace, P.J., 2013. Why do mafic arc magmas contain ~4 wt% water on average? Earth Planet. Sci. Lett. 364, 168-179. https://doi.org/10.1016/j.epsl.2012.11.044

Ponomareva, V.V., Kyle P., Pevzner, M. M. et al., 2007. Holocene Eruptive History of Shiveluch Volcano, Kamchatka Peninsula, Russia. In: Volcanism and Subduction: The Kamchatka region // (Eichelberger J., Gordeev E., Izbekov P., Lees J. Eds), AGU Geophysical Monograph. 172: 263-282.

Ponomareva, V., Portnyagin, M., Pevzner, M., et al., 2015. Tephra from andesitic Shiveluch volcano, Kamchatka, NW Pacific: Chronology of explosive eruptions and geochemical

fingerprinting of volcanic glass. International Journal of Earth Sciences. 104: 1459-1482. https://doi.org/10.1007/s00531-015-1156-4

Portnyagin, M.V., Hoernle, K., Plechov, P.Y., Mironov, N.L., Khubunaya, S.A., 2007. Constraints on mantle melting and composition and nature of slab components in volcanic arcs from volatiles (H_2O, S, Cl, F) and trace elements in melt inclusions from the Kamchatka Arc. Earth Planet. Sci. Lett. 255, 53-69. https://doi.org/10.1016/j.epsl.2006.12.005

Portnyagin, M. V., Ponomareva, V. V., Zelenin, E.A., Bazanova, L.I., Pevzner, M.M., Plechova, A.A., Rogozin, A.N., Garbe-Schönberg, Di., 2020. TephraKam: Geochemical database of glass compositions in tephra and welded tuffs from the Kamchatka volcanic arc (northwestern Pacific). Earth Syst. Sci. Data 12, 469–480. https://doi.org/10.5194/essd-12-469-2020

Putirka, K., 2016. Amphibole thermometers and barometers for igneous systems and some implications for eruption mechanisms of felsic magmas at arc volcanoes. American Mineralogist, 101(4): 841-858. https://doi.org/10.2138/am-2016-5506

Ramsey, Michael S., Wessels, Rick L., Anderson, Steven W., 2012. Surface textures and dynamics of the 2005 lava dome at Shiveluch volcano, Kamchatka. GSA Bulletin. 124 (5-6): 678–689. doi: https://doi.org/10.1130/B30580.1

Ridolfi F, Renzulli A, Puerini M., 2010. Stability and chemical equilibrium of amphibole in calc-alkaline magmas: an overview, new thermobarometric formulations and application to subduction-related volcanoes. Contributions to Mineralogy and Petrology.160: 45-66. https://doi.org/10.1007/s00410-009-0465-7

Ridolfi, F., & Renzulli, A., 2012. Calcic amphiboles in calc-alkaline and alkaline magmas: thermobarometric and chemometric empirical equations valid up to 1,130° C and 2.2 GPa. Contributions to Mineralogy and Petrology, 163(5), 877-895. https://doi.org/10.1007/s00410-011-0704-6

Ridolfi, F., Braga, R., Cesare, B., Renzulli, A., Perugini, D. and Del Moro, S., 2016. Unravelling the complex interaction between mantle and crustal magmas encoded in the lavas of San Vincenzo (Tuscany, Italy). Part I: Petrography and Thermobarometry. Lithos, 244, 218-232. https://doi.org/10.1016/j.lithos.2015.09.029

Ridolfi, F., Zanetti, A., Renzulli, A., Perugini, D., Holtz, F. and Oberti, R., 2018. AMFORM, a new mass-based model for the calculation of the unit formula of amphiboles from electron microprobe analyses. American Mineralogist: Journal of Earth and Planetary Materials, 103 (7);1112-1125. https://doi.org/10.2138/am-2018-6385

Rutherford M. J., Devine J. D., 2003. Magmatic conditions and magma ascent as indicated by hornblende phase equilibria and reactions in the 1995–2002 Soufrie`re Hills magma. Journal of Petrology. 44 (8): 1433–1453.

Ruprecht, P., & Bachmann, O., 2010. Pre-eruptive reheating during magma mixing at Quizapu volcano and the implications for the explosiveness of silicic arc volcanoes Geology 38(10):919-922 DOI: 10.1130/G31110.1

Ruprecht, P., Bergantz, G. W., Cooper, K. M., Hildreth, W., 2012. The crustal magma storage system of Volcán Quizapu, Chile, and the effects of magma mixing on magma diversity. Journal of Petrology, 53(4): 801-840. https://doi.org/10.1093/petrology/egs002

Ruprecht, P., Simon, A.C. and Fiege, A., 2020. The Survival of Mafic Magmatic Enclaves and the Timing of Magma Recharge. Geophysical Research Letters, 47(14), p.e2020GL087186.

Sato, H., Holtz, F., Behrens, H., Botcharnikov, R., & Nakada, S., 2005. Experimental petrology of the 1991–1995 Unzen dacite, Japan. Part II: Cl/OH partitioning between hornblende and melt and its implications for the origin of oscillatory zoning of hornblende phenocrysts. Journal of Petrology. 46(2): 339-354. https://doi.org/10.1093/petrology/egh078

Scaillet B. and Evans B., 1999. The 15 June 1991 eruption of Mount Pinatubo. I. Phase equilibria and pre-eruption P–T–fO_2–H_2O conditions of the dacite magma. Journal of Petrology. 40 (3): 381-411.

Schmidt, M.W., 1992. Amphibole composition in tonalite as a function of pressure: An experimental calibration of the Al-in-hornblende barometer. Contribution to Mineralogy and Petrology. 110 (2-3): 304- 310.

Simakin, A. G., Salova, T. P., & Babansky, A. D., 2009. Amphibole crystallization from a water-saturated andesite melt: Experimental data at P= 2 kbar. Petrology. 17(6): 591. https://doi.org/10.1134/S086959110906006X

Simakin A.G., Shaposhnikova O. Yu., 2017. Novel amphibole geobarometer for high-magnesium andesite and basalt magmas // Petrology. 25 (2): 226–240. https://doi.org/10.1134/S0869591117020047

Shcherbakov, V. D., Plechov, P. Y., Izbekov, P. E., & Shipman, J. S., 2011. Plagioclase zoning as an indicator of magma processes at Bezymianny Volcano, Kamchatka. Contributions to Mineralogy and Petrology, 162(1): 83-99. https://doi.org/10.1007/s00410-010-0584-1

Shevchenko A.V., Dvigalo V.N., Svirid I.Yu., 2015. Airborne photogrammetry and geomorphological analysis of the 2001–2012 exogenous dome growth at Molodoy

Shiveluch Volcano, Kamchatka. Journal of Volcanology and Geothermal Research. 304: 94-107. https://doi.org/10.1016/j.jvolgeores.2015.08.013

Sparks R. S. J., Sigurdsson H., Wilson L., 1977. Magma mixing—mechanism for triggering acid explosive eruptions. Nature. 267: 315–318.

Sparks R. S. J., 1997. Causes and consequences of pressurisation in lava dome eruptions. Earth and Planetary Science Letters. 150 (3-4): 177-189.

Spear, F. S., 1981. An experimental study of hornblende stability and compositional variability in amphibolite. American Journal of Science. 281(6): 697-734.

Streck Martin J.; Mineral Textures and Zoning as Evidence for Open System Processes. Reviews in Mineralogy and Geochemistry ; 69 (1): 595–622. doi: https://doi.org/10.2138/rmg.2008.69.15

Thornber, C.R., Pallister, J.S., Lowers, H.A., Rowe, M.C., Mandeville, C.W., Meeker, G.P., 2008. Chapter 32. Chemistry, mineralogy, and petrology of amphibole in Mount St. Helens 2004–2006 dacite. U.S. Geological Survey Professional Paper: 727–754.

Tobelko, D.P., Portnyagin, M.V., Krasheninnikov, S.P., Grib, E.N., Plechov, P.Y., 2019. Composition and conditions of primitive magma origin of Karymsky volcanic center (Kamchatka) estimated using melt inclusions and trace element thermobarometry. Petrology (27): 259-282, https://doi.org/210.31857/S30869-5903273258-5903273281.

Tokarev, P. I., 1967. Gigantic eruption of Shiveluch volcano on 12 November 1964 and its precursors. Izv. AN SSSR Phys. Earth, 9: 11-22 (In Russian).

Tolstykh, M. L., Naumov, V. B., Khubunaya, S. A., et al., 1998. The melt composition and crystallization conditions of andesites from Shiveluch volcano in Kamchatka: evidence from mineral hosted inclusions // Doklady Earth Sciences. 359 (3): 440-443.

Tolstykh, M. L., Naumov, V. B., Babansky, A. D., et al., 2003. Chemical Composition, Volatile Components, and Trace Elements in Andesitic Magmas of the Kurile-Kamchatka Region Petrology. 11 (5): 407-425.

Turner, S. J., Izbekov, P., & Langmuir, C., 2013. The magma plumbing system of Bezymianny Volcano: Insights from a 54 year time series of trace element whole-rock geochemistry and amphibole compositions. Journal of Volcanology and Geothermal Research. 263: 108-121. https://doi.org/10.1016/j.jvolgeores.2012.12.014

Volynets, O. N., Ponomareva, V.V., Babansky, A. D., 1997. Magnesian basalts of Shiveluch andesite volcano, Kamchatka. Petrology 5(2): 183-196

Wanke, M., Karakas, O., & Bachmann, O., 2019. The genesis of arc dacites: the case of Mount St. Helens, WA. Contributions to Mineralogy and Petrology, 174(1): 7. https://doi.org/10.1007/s00410-018-1542-6

Whitney, D. L., & Evans, B. W., 2010. Abbreviations for names of rock-forming minerals. American mineralogist, 95(1): 185-187.

Witter J. B., Kress V. C., Newhall C. G., 2005. Volcán Popocatépetl, Mexico. Petrology, Magma Mixing, and Immediate Sources of Volatiles for the 1994–Present Eruption. Journal of Petrology, 46 (11): 2337–2366. https://doi.org/10.1093/petrology/egi058

Zhang, J., Humphreys, M. C., Cooper, G. F., Davidson, J. P., & Macpherson, C. G., 2017. Magma mush chemistry at subduction zones, revealed by new melt major element inversion from calcic amphiboles. American Mineralogist: Journal of Earth and Planetary Materials, 102(6): 1353-1367. https://doi.org/10.2138/am-2017-5928

Zharinov, N. A., Bogoyavlenskaya G. E., Khubunaya, S. A., Demyanchuk, Yu.V., 1995. A new eruption cycle of Shiveluch volcano, 1980-1993. Volcanol Seismol. 17: 21-30.

Zharinov, N. A., & Demyanchuk, Y. V., 2013. Large explosive eruptions of Shiveluch volcano, Kamchatka resulting in partial destruction of the extrusive dome (February 28, 2005 and October 27, 2010). Journal of Volcanology and Seismology. 7(2):131-144.

Zobin, V.M, 1971. Mechanism of volcanic earthquakes at Sheveluch Volcano, Kamchatka Bulletine of Volcanology. 35(1): 225-242.

Fig. 1. Shiveluch volcanic massif.

(a) A view of Shiveluch volcano from the south on July, 31, 2015. Photo by Anastasiya Plechova. (b) Location of Shiveluch in Kamchatka. CKD - Central Kamchaka depression; KGV - Kliuchevskaya volcanic group; SH - Shiveluch volcanic massif. (c) Major structural units of Shiveluch volcano and distribution of the most voluminous recent pyroclastic deposits. Small dots in (c) denote locations illustrated by photos in Fig. 2.

Fig. 2. Growing Shiveluch dome and its eruptive products.

(a) Dome in September, 28, 2016; (b) Pyroclastic flow deposits of the February, 2005 eruption at a distance of 10 km from the eruptive center; (c) Pyroclastic deposits of October, 2010 eruption as seen at a distance of 13 km from the eruption center. (d) Large andesite block from the 2005 pyroclastic deposits that contains mafic enclaves (shown in the inset). (e) One of the latest pyroclastic flows in the September, 2016.

Fig. 3. Photomicrographs (cross polarized light) of the Shiveluch rocks.

(a) Pumice of 1964 plinian eruption; (b) Massive andesite from block in 2016 pyroclastic flow; (c) Andesite with opacitized amphibole crystals from the early episode of the lava dome

growth in 1993-1995; (d) Olivine crystal mantled by an *Opx-Hbl* reaction rim from 2016 andesite; (e) Contact zone between mafic enclave and host andesite erupted in February 2005; (f) Inner part of an enclave with olivine and amphibole phenocrysts and fine-grained matrix.

Fig. 4. Composition of recently erupted Shiveluch rocks.

(a) SiO_2 vs. Na_2O+K_2O diagram for Shiveluch rocks, melt inclusions and matrix glasses; (b) Temporal variations of SiO_2 contents in Shiveluch rocks and matrix glasses. The compositions of Holocene Young Shiveluch rocks (Ponomareva et al., 2007 and Gorbach and Portnyagin, 2011), melt inclusions and matrix glasses (Tolstykh, 1998; 2003; Humphreys et al., 2008; Ponomareva et al., 2015) are shown for comparison.

Fig. 5. N-MORB-normalized trace element patterns (a) and Cl-chondrite-normalized REE abundances (b) for the Shiveluch dome andesite, mafic enclaves and pumice of 1964 plinian eruption. N-MORB and Cl-chondrite values are after Sun and McDonough (1989).

Fig. 6. Appearance and composition of amphiboles in Shiveluch andesites and associated mafic enclaves:

(a) – phenocrysts of low-Al magnesiohornblende (*Mhb)* (10.5 and 8.3 wt.% Al_2O_3 in core and rim, respectively) associated with apatite (*Ap*) and (*Mt*) grains; (b) – phenocryst with patchy core (Al_2O_3~11 wt.%) rimmed by a concentric zone with abundant inclusions of plagioclase (*Pl*), magnetite (*Mt*) and glass; (c) – opacitized low-Al *Mhb* crystal with *Pl*, *Ap*, *Opx* and *Mt* inclusions from an early episode of the dome growth in 1993-1995; (d) – basaltic andesite enclave - host andesite contact zone with crystals of high-Al magnesiohastingsite (*Mhs*) (Al_2O_3~11-14 wt.%) in an enclave and low-Al *Mhb* surrounded by the rim of *Mhs* in andesite; (e) – resorbed crystal with core comprising patches of low-Al (Al_2O_3~7-8 wt.%) and high-Al (Al_2O_3~10-11 wt.%) pargasite amphibole; (f) – cloth of crystals with high-Al cores (Al_2O_3~12.5 wt.%) and low-Al (Al_2O_3~7-8 wt.%) rims; (g, h) – amphiboles from different Shiveluch eruptions plotted on classification amphibole diagrams (Leake et al., 1997)

Fig. 7. Chemical composition (a, b) of amphiboles and cations substitutions (c-f).

(a) – MgO-Al_2O_3 and (b) – MgO-Cl variation diagrams; (c) – pressure-sensitive Al-Tschermak-type ($2Si^{IV}+Mg^{VI}=2Al^{IV}+Al^{VI}$) exchange; (d) – temperature-sensitive edenite-type ($Si^{IV}+()^{A}=Al^{IV}+(Na+K)^{A}$ exchange; (e) – temperature-sensitive Ti-Tschermak ($2Si^{IV} + Mn^{VI} = 2Al^{IV} + Ti^{VI}$) exchange; (f) – temperature-sensitive plagioclase-type ($Si^{IV} + Na^{A} = Al^{IV} + Ca^{A}$)

exchange. Al_2O_3, MgO and Cl are given in wt. %, cations in atoms per formula unit (a.p.f.u.). Cation abundances are calculated based on 13 cation model (Leake et al., 1997).

Fig. 8. Major types of amphibole phenocrysts from the 1964 plinian eruption (a, b) and the early period of lava dome growth in 1993-1995 (c). The plot illustrates BSE images and compositional parameters (MgO, Al_2O_3, Al^{IV}, Mg#, $(Na+K)^A$ and Al^{VI} abundances) for representative phenocrysts. Mg# is given as Mg/Mg+Fe assuming that all Fe is Fe^{2+}.
Parts of crystals that were selected for thermobarometric calculations are shown by gray pattern.

Fig. 9. Amphibole crystals from a mafic enclave (a), its contact with the host andesite (b), and from an andesite of one of the latest Shiveluch eruptions in 2013 (c). The plot illustrates BSE images and compositional parameters (MgO, Al_2O_3, Al^{IV}, Mg#, $(Na+K)^A$ and Al^{VI} abundances) for representative phenocrysts. Mg# is given as Mg/Mg+Fe assuming that all Fe is Fe^{2+}. Parts of crystals that were selected for thermobarometric calculations are shown by gray pattern.

Fig. 10. Conditions of amphibole crystallization:
(a) – *P-T* diagram showing temperature estimates using the model of Putirka (2016) and pressure after Ridolfi and Renzulli (2012). Additional pressure estimations for mafic amphiboles using the approach of Simakin and Shaposhnikova (2017) are shown with white circles. Experimental amphibole composition produced at 500 MPa and 990 ^oC by Simakin and Shaposhnikova (2017) is shown by yellow star. The lower and upper thermal stability limits of amphibole are shown by dashed and dotted lines, respectively. Green lines denote SiO_2 content in melt coexisting with amphibole (modified after Ridolfi et al., 2010); (b) – amphibole crystallization temperatures (model by Putirka, 2016) for different periods of the recent Shiveluch activity. The uncertainties of the mean values correspond to 2σ.

Fig. 11. A schematic model of the magmatic plumbing system of Shiveluch volcano based on the interpretation of amphibole compositions.
Dark grey crystals are high-Al *Mhs* crystallized at high pressure in the low-to-middle crust magma storage zone. Light grey crystals correspond to low-Al *Mhb* crystallizing at low pressure in the shallow magma reservoir. Patchy and simple types of amphibole zoning are formed during ascent of magma to the shallow magma chamber. Simple zoning results from

magma cooling and crystallisation processes. Amphiboles with reverse zoning indicate replenishments of the shallow magma reservoir with mafic magma from depth.

Table 1. Representative major and trace elements compositions of Shiveluch andesites and mafic enclaves

Eruption	**1964**	**1964**	**2001**	**2004**	**2005**	**2005**	**2007**	**2013**	**2013**	**2013**	**2016**
Sample#	7662-1	7662-2	3000-1	7433	7452-1	7499-4	7515	7637-2	7661-1	7661-2	7685-1
	Pumice	Pumice	Pumiceous clast from PF	Dome	Dome	Enclave	Dense block from PF	Pumiceous clast from PF	Dense block from PF	Enclave	Dense block from PF
SiO_2	60.56	61.92	61.35	62.74	62.65	56.30	63.48	62.26	63.11	54.85	60.16
TiO_2	0.55	0.50	0.54	0.52	0.51	0.59	0.48	0.46	0.46	0.69	0.56
Al_2O_3	16.32	16.82	16.48	16.57	16.65	15.46	16.49	16.65	16.65	15.43	15.75
FeO^{tot}	5.02	4.37	4.59	4.44	4.45	6.30	4.28	4.58	3.97	6.88	5.15
MnO	0.10	0.09	0.09	0.09	0.09	0.11	0.09	0.09	0.08	0.13	0.10
MgO	4.11	3.42	3.58	3.45	3.49	7.82	3.3[illegible]	3.30	3.28	8.20	4.74
CaO	6.02	5.68	5.76	5.51	5.64	7.49	5.38	5.42	5.41	8.07	6.07
Na_2O	4.43	4.81	4.77	4.88	4.84	3.74	[illegible].90	4.95	4.87	3.60	4.56
K_2O	1.33	1.24	1.24	1.20	1.24	0.97	[illegible].25	1.19	1.25	0.78	1.32
P_2O_5	0.16	0.14	0.16	0.15	0.16	0.13	[illegible].15	0.14	0.13	0.14	0.17
H_2O	0.60	0.30	0.79	0.29	0.23	0.46	0.[illegible]6	0.06	0.10	0.10	1.17
CO_2	n.d.	n.d.	0.02	0.04	0.01	0.05	[illegible].00	n.d.	n.d.	n.d.	n.d.
Total	99.20	99.29	99.35	99.84	99.95	99.37	99.98	99.10	99.31	98.87	99.76
Mg#	0.59	0.58	0.58	0.58	0.58	0.[illegible]69	0.58	0.56	0.60	0.68	0.62
Li	15	13	n.d.	n.d.	18	15	n.d.	n.d.	n.d.	n.d.	18
Sc	15	13	n.d.	n.d.	17	[illegible]1	n.d.	n.d.	12	25	18
V*	126	113	119	114	110	178	106	106	104	195	139
Cr*	144	103	108	110	118	[illegible]74	114	157	103	438	174
Co*	18	15	20	15	[illegible]	35	15	13	15	33	21
Ni*	40	32	18	18	16	110	14	11	30	125	49
Cu	n.d.	n.d.	n.d.	n.d.	[illegible]6	98	n.d.	11	n.d.	n.d.	33
Zn*	n.d.	n.d.	60	56	52	60	54	17	n.d.	n.d.	62
Ga*	17	17	18	18	[illegible]8	17	17	18	18	16	19
Rb*	23	20	24	24	24	18	26	21	22	13	25
Sr*	611	655	557	569	579	451	567	622	633	502	566
Y*	13	11	12	[illegible]3	10	12	12	10	10	15	15
Zr*	108	97	97	9[illegible]	93	68	93	90	95	83	91
Nb	2.00	1.50	n.d.	[illegible].d.	1.69	1.17	n.d.	1.40	1.50	1.50	2.46
Mo	n.d.	n.d.	n.d.	n.d.	1.15	0.86	n.d.	0.20	n.d.	n.d.	1.09
Sn	n.d.	n.d.	n.d.	n.d.	0.61	0.58	n.d.	<1	<1	<1	0.85
Sb	n.d.	n.d.	n.d.	n.d.	0.52	0.32	n.d.	n.d.	n.d.	n.d.	1.20
Cs	0.80	0.80	n.d.	n.d.	0.82	0.57	n.d.	0.90	0.70	0.40	0.99
Ba*	437	413	37[illegible]	387	390	296	399	427	450	278	439
La	8.50	7.40	n.[illegible]	n.d.	7.19	4.98	n.d.	8.50	8.00	6.20	8.91
Ce	19.60	16.20	n.d.	n.d.	16.44	12.03	n.d.	15.10	16.30	15.30	20.73
Pr	2.63	2.24	n.d.	n.d.	2.35	1.81	n.d.	2.16	2.15	2.15	2.91
Nd	11.70	10.20	n.d.	n.d.	10.34	8.48	n.d.	10.40	9.60	10.50	12.69
Sm	2.73	2.18	n.d.	n.d.	2.41	2.22	n.d.	2.10	2.20	2.60	3.02
Eu	0.82	0.69	n.d.	n.d.	0.76	0.73	n.d.	0.76	0.68	0.83	0.94
Gd	2.62	2.27	n.d.	n.d.	2.34	2.30	n.d.	2.13	2.14	2.78	2.82
Tb	0.40	0.34	n.d.	n.d.	0.35	0.36	n.d.	0.28	0.32	0.44	0.42
Dy	2.31	1.91	n.d.	n.d.	2.00	2.17	n.d.	1.68	1.86	2.69	2.57
Ho	0.42	0.37	n.d.	n.d.	0.40	0.45	n.d.	0.35	0.36	0.57	0.54
Er	1.30	1.13	n.d.	n.d.	1.10	1.23	n.d.	0.98	1.04	1.63	1.44
Tm	0.19	0.16	n.d.	n.d.	0.17	0.18	n.d.	0.14	0.14	0.23	0.22
Yb	1.31	1.11	n.d.	n.d.	1.11	1.21	n.d.	0.93	1.02	1.58	1.38
Lu	0.20	0.17	n.d.	n.d.	0.17	0.18	n.d.	0.15	0.17	0.22	0.21
Hf	2.70	2.70	n.d.	n.d.	2.46	1.99	n.d.	2.40	2.50	2.20	2.54
Ta	0.10	0.10	n.d.	n.d.	0.13	0.08	n.d.	0.10	0.10	<0.1	0.17
W	n.d.	n.d.	n.d.	n.d.	0.19	0.12	n.d.	<0.5	<0.5	<0.5	0.28
Tl	n.d.	n.d.	n.d.	n.d.	0.12	0.14	n.d.	n.d.	n.d.	n.d.	0.23
Pb	n.d.	n.d.	n.d.	n.d.	4.73	3.65	n.d.	n.d.	n.d.	n.d.	6.41
Th	0.90	0.80	n.d.	n.d.	0.99	0.62	n.d.	1.00	0.70	0.50	1.20
U	0.50	0.40	n.d.	n.d.	0.57	0.34	n.d.	0.60	0.50	0.30	0.68
Lab	Acme	Acme	Kiel	Kiel	Kiel	Kiel	Kiel	Acme	Acme	Acme	Irkutsk

Note: Major elements (in wt. %) and trace elements (in ppm) marked with an asterisk were obtained by the X-ray fluorescence method; other trace elements were analyzed by ICP-MS; PF - pyroclastic flow.

Table 2. Representative compositions and physicochemical conditions for amphiboles from different Shiveluch eruptions

Eruption	**1964**				**1993**				**2001**				**2004**			
Occurrence	Pumice				Dome				Pumiceous 3001				Dome			
Sample#	7662-1				1993-1								7433			
Type of zoning	**Patchy**		**Simple**		**Weakly zoned**		**Simple**		**Unzoned**		**Simple**		**Patchy**		**Simple**	
Position	core	rim	core	rim	core	rim	core	rim	core	rim	core	rim	core	rim	core	rim
Phase	*Mhs*	*Mhb*	*Mhs*	*Mhb*	*Mhb*	*Mhb*	*Mhs*	*Mhb*	*Mhb*	*Mhb*	*Mhb*	*Mhb*	*Mhs*	*Mhb*	*Prg*	*Mhb*
	1	2	3	4	5	6	7	8	9	10	11	12	13	14	15	16
SiO_2	42.92	47.30	42.39	48.39	45.96	46.62	43.63	46.92	45.73	45.68	44.88	47.64	40.72	45.24	43.47	46.39
TiO_2	1.42	1.76	1.75	1.49	2.02	1.85	2.46	2.04	1.79	2.00	2.76	1.75	2.02	1.80	2.53	1.96
Al_2O_3	12.47	7.86	13.20	7.36	8.65	8.05	10.53	7.82	9.29	9.07	9.55	7.81	12.78	9.27	10.39	7.97
FeO^{tot}	12.87	11.11	12.94	10.66	12.16	12.04	12.72	11.41	12.38	12.66	12.38	11.50	14.28	13.10	14.14	12.60
MnO	0.25	0.27	0.22	0.32	0.26	0.26	0.29	0.28	0.30	0.30	0.30	0.18	0.20	0.17	0.19	0.26
MgO	13.64	15.85	12.76	16.33	14.99	15.28	13.95	15.49	15.09	14.86	14.28	15.77	13.27	14.96	13.32	15.34
CaO	11.38	11.42	11.69	11.26	11.33	11.34	11.49	11.58	11.20	11.03	11.29	11.04	11.25	10.93	10.96	10.88
Na_2O	2.39	1.83	2.33	1.63	2.07	1.96	2.38	1.88	1.98	2.12	2.34	1.81	2.96	1.99	2.55	2.01
K_2O	0.43	0.31	0.59	0.27	0.39	0.38	0.57	0.37	0.40	0.48	0.52	0.35	0.45	0.44	0.46	0.46
Cr_2O_3	0.06	0.11	0.03	0.06	0.02	0.03	0.03	0.04	0.00	0.00	0.00	0.00	0.00	0.00	0.00	0.00
Cl	0.03	0.06	0.03	0.03	0.06	0.06	0.07	0.05	n.d.	n.d.	n.d.	n.d.	n.d.	n.d.	n.d.	n.d.
Total	97.86	97.88	97.93	97.81	97.93	97.38	98.02	97.86	97.86	97.91	98.02	97.84	97.91	97.89	98.00	97.86
Mg#	0.65	0.72	0.64	0.73	0.69	0.69	0.66	0.71	0.68	0.68	0.67	0.71	0.62	0.67	0.63	0.68
Physicochemical conditions for homogenous parts of crystals																
T°[C]	936	868	940	845	882	872	n.h.	n.h.	887	888	n.h.	863	n.h.	887	918	884
P[MPa]	397	142	445	127	181	139	n.h.	n.h.	170	166	n.h.	116	n.h.	207	281	136
P_{max}[MPa]	469		535													
ΔNNO	0.94	1.69	0.48	1.95	1.48	1.51	n.h.	n.h.	1.48	1.36	n.h.	1.73	n.h.	1.53	0.69	1.64
H_2O, wt.%	7.17	4.62	7.69	4.71	4.44	4.47	n.h.	n.h.	5.13	4.66	n.h.	4.59	n.h.	4.83	5.21	4.05

Table 2. Continue

Eruption	**2005**				**2005**				**2007**				**2013**					
Occurrence	Enclave 7499-4				Enclave-host andesite contact				Dome				Pumiceuos					
Sample#					7499-4a				7522				7537-2					
Type of zoning	**Weakly zoned**		**Weakly zoned**		**Reverse 1**		**Reverse 1**		**Simple**		**Patchy**		**Reverse 2**		**Simple**		**Simple (cloths)**	
Position	core	rim	zone	rim	core	rim	core	rim	core	rim	core	rim	core	rim	core	rim	core	rim
Phase	*Mhs*	*Mhs*	*Mhs*	*Mhs*	*Mhb*	*Mhs*	*Mhb*	*Mhs*	*Mhs*	*Mhb*	*Mhs*	*Mhb*	*Mhb*	*Mhb*	*Prg*	*Mhb*	*Mhs*	*Mhb*
	17	18	19	20	21	22	23	24	25	26	27	28	29	30	31	32	33	34
SiO_2	42.	42.	43.	43.	47.2	42.	46.	41.	42.	46.7	43.	45.	47.5	46.	44.	47.	42.	46.
TiO_2	1.9	2.4	1.5	1.4	1.64	1.4	1.8	2.3	1.9	2.05	1.7	1.5	1.75	1.2	1.6	1.8	2.0	1.8
Al_2O_3	13.	12.	12.	12.	8.02	13.	8.5	12.	12.	7.96	12.	9.1	7.45	9.7	10.	7.6	12.	8.4
FeO^{tot}	10.	12.	8.9	9.9	11.4	12.	11.	12.	10.	11.3	9.7	11.	11.6	7.9	12.	11.	13.	11.
MnO	0.1	0.1	0.1	0.1	0.25	0.2	0.2	0.1	0.1	0.29	0.2	0.2	0.28	0.0	0.2	0.2	0.2	0.3
MgO	15.	13.	16.	15.	15.5	13.	15.	13.	15.	15.9	15.	15.	15.6	17.	14.	15.	13.	15.
CaO	11.	11.	11.	11.	11.4	11.	11.	11.	11.	11.5	11.	11.	11.4	12.	11.	11.	11.	11.
Na_2O	2.6	2.8	2.5	2.4	1.78	2.3	1.9	2.7	2.4	1.79	2.4	1.9	1.76	2.1	2.1	1.7	2.3	1.9
K_2O	0.3	0.3	0.3	0.3	0.35	0.5	0.3	0.3	0.4	0.3	0.4	0.3	0.31	0.1	0.5	0.3	0.4	0.3
Cr_2O_3	0.0	0.0	0.1	0.0	0.02	0.0	0.0	0.0	0.0	0.01	0.1	0.2	0.04	0.0	0.1	0.0	0.0	0.0
Cl	0.0	0.0	0.0	0.0	0.05	0.0	0.0	0.0	n.d	n.d	n.d	n.d	0.07	0.0	0.0	0.0	0.0	0.0
Total	97.	97.	97.	97.	97.8	97.	97.	98.	97.	97.9	97.	97.	97.8	97.	97.	97.	97.	97.
Mg#	0.7	0.6	0.7	0.7	0.71	0.6	0.7	0.6	0.7	0.71	0.7	0.7	0.71	0.8	0.6	0.7	0.6	0.6
Physicochemical conditions for homogenous parts of crystals																		
T°[C]	98	97	97	96	861	n	88	.	98	878	n.	89	856	n.	90	85	94	88
P[MPa]	46	38	43	36	132	n	1	n.	46	146	n.	22	109	n.	31	12	41	17
P_{max}[M	55		46															
ΔNNO	1.0	0.7	1.5	1.3	1.62	n.	1.5	n.	1.3	1.67	n.	1.6	1.66	n.	1.0	1.5	0.6	1.4
H_2O,	7.1	6.0	6.6	6.7	4.89	n.	4.6	n.	6.0	4.38	n.	4.9	4.56	n.	6.0	4.8	7.0	4.8

Note. The check of stoichiometry and mi or correction of the amphibole microprobe analyses were performed using the AMFORM model (Ridolfi et al., 2018).
Mg# is given as Mg/Mg+Fe assuming that all Fe is Fe^{2+};
n. h. indicates not homogeneous parts of crystals which are not suitable for thermobarometric calculations according (Gorini et al., 2018).
The crystallization temperatures (*T*) recalculated using the model of Putirka (2016); pressure (*P*) by Ridolfi, and Renzulli (2012) and (P_{max}) by Simakin and Shaposhnikova, 2017; oxygen fugacity (ΔNNO) and melt H_2O contents calculated using the approach by Ridolfi et al. (2010).

Highlights

- Detailed analysis of Shiveluch volcano activity from 1964 to present time.
- Amphibole composition correlates with year and style of eruption, and depicts variable paths of magma fractionation.
- Amphibole phenocrysts crystallized in two magma storage zones at 15-20 km and 5-6 km under volcano.
- Parental Shiveluch magmas are the most hydrous on Kamchatka and contained up to 8 wt% H_2O.